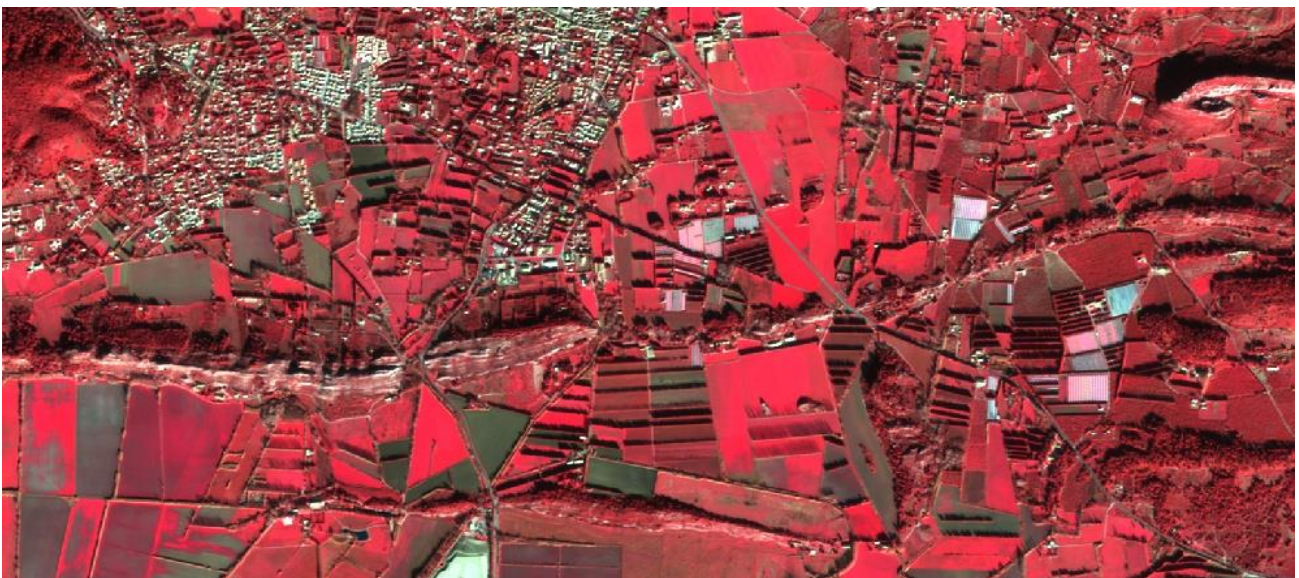# JRC TECHNICAL REPORTS

Geometry Benchmark of DEIMOS-2 for the CAP Control with Remote Sensing

Geometric benchmarking over Maussane test site for the Common Agriculture Policy

deimosimaging
an urthecast company

AIRBUS
DEFENCE & SPACE

Blanka Vajsová
Cristina Moclán
Pär Johan Åstrand
Roberto Fabrizi
2016

This publication is a Technical report by the Joint Research Centre (JRC), the European Commission's science and knowledge service. It aims to provide evidence-based scientific support to the European policy-making process. The scientific output expressed does not imply a policy position of the European Commission. Neither the European Commission nor any person acting on behalf of the Commission is responsible for the use which might be made of this publication.

Contact information
Name: Pär Johan Åstrand
Address: Joint Research Centre, Via Enrico Fermi 2749, TP 263, 21027 Ispra (VA), Italy
E-mail: par-johan.astrand@jrc.ec.europa.eu
Tel.:   +39 0332 78 6215

Table of contents

Abstract

The main objective of the present study is to assess whether DEIMOS-2 sensor can be recomended for Control with Remote Sensing program (CwRS), in Common Agriculture Policy (CAP).

The benchmarking presented herein aims at evaluating the usability of DEIMOS-2 for the CAP checks through an estimation of its geometric (positional) accuracy, as well as measuring the influence of different factors (viewing angle, number of GCPs, software implementation) on this accuracy.

The planimetric accuracy of the DEIMOS-2 orthoimagery, expressed as the 1D RMSE measured on Check Points in both Easting and Northing directions, is below the 5 m scale geometric specification required for the CAP HHR profile defined in the HR profile based technical specifications.

1 Introduction

The main objective of the present study is to assess whether DEIMOS-2 sensor can be qualified for Control with Remote Sensing program (CwRS), in Common Agriculture Policy (CAP).

The EU standard for the orthoimagery to be used for the purpose of Common Agriculture Policy (CAP) checks requires appropriate quality of the input data, as well as the quality assessment of the final orthoimagery. Within this context, the objective of the current study is to perform an initial quality assessment of the geometric capabilities of the DEIMOS-2 satellite.

In order to fulfil Control with Remote Sensing (CwRS) requirements, it has been proposed to assess the geometric accuracy of DEIMOS-2 products. Several PSH, PAN and MS4 products have been generated from DEIMOS-2 raw images over the AOI. Different GCP configurations and processing platforms have been used and their results have been compared.

2 DEIMOS-2 System

DEIMOS-2 is a very-high resolution multispectral optical satellite, fully owned and operated by Deimos Imaging, an UrtheCast company. The DEIMOS-2 end-to-end system has been designed to provide a cost-effective yet highly responsive service to customers worldwide.

DEIMOS-2 is the second satellite of the DEIMOS Earth Observation system, following the DEIMOS-1, which was launched in 2009 and provides mid-resolution, very-wide-swath imagery.

DEIMOS-2 has been launched on June 19, 2014, with a mission lifetime of at least seven years. It operates from a Sun-synchronous orbit at a mean altitude of 620 km, with a local time of ascending node (LTAN) of 10h30, which allows an average revisit time of two days worldwide (one day at mid-latitudes).

The spacecraft design is based on an agile platform for fast and precise off-nadir imaging (up to ±30º over nominal scenarios and up to ±45º in emergency cases), and it carries a push-broom very-high resolution camera with 5 spectral channels (1 panchromatic, 4 multispectral).

Deimos Imaging manages all uplink and downlink activities, as well as satellite control and image processing and archiving facilities. DEIMOS-2 makes use of four ground stations located in Puertollano and Boecillo (Spain), Kiruna (Sweden) and Inuvik (Canada) in order to maximise redundancy and availability, and to guarantee at least one contact with the satellite at each orbit. Secondary ground stations could be used for uplink and downlink activities, thus allowing an even better performance in terms of response time and imaging capabilities.
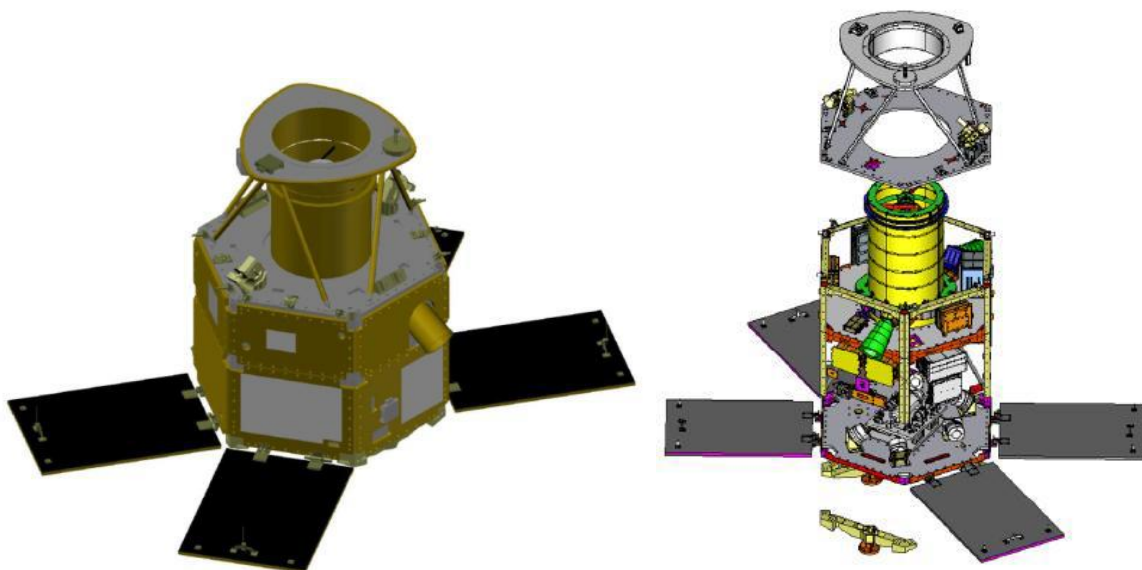

Figure 1: External and cutaway views of the DEIMOS-2 satellite

The following table summarize the main characteristics of DEIMOS-2:

Satellite name	DEIMOS-2
International designations	2014-033D / 40013 (NORAD)
Date of launch	June 19, 2014
Expected lifetime	At least 7 years
Orbit altitude	620 km (Sun-Synchronous)
Local time at ascending node	10:30 (ascending orbit)
Average revisit time	2 days worldwide (with ±45º viewing angle)
Sensor name	HiRAIS / EOS-D
Sensor type	Optical
Bands and spectral ranges	λ @ FWHM (nm) <table><tr><td></td><td>min</td><td>max</td></tr><tr><td>PAN</td><td>560</td><td>900</td></tr><tr><td>Blue</td><td>466</td><td>525</td></tr><tr><td>Green</td><td>532</td><td>599</td></tr><tr><td>Red</td><td>640</td><td>697</td></tr><tr><td>NIR</td><td>770</td><td>892</td></tr></table>
Spatial resolution	PAN/Pan-sharpened on nadir conditions: • 1 m GSD (PAN) Multispectral: • 4 m GSD (Multispectral bands)
Depth of imaging (bits of radiometric resolution)	10
Swath width	12 km
Along-track imaging capacity	Up to 1,400 km
Viewing/incidence angles	Agile platform allows up to ±30º pitch and ±45º roll down emergency scenarios
Geometric accuracy	100 m CE90 without GCP
Stereo-pair capacity	Capable of single-pass stereo-pair acquisitions
System capacity	Up to 200,000 km2 per day

Table 1: DEIMOS-2 main characteristics

2.1 DEIMOS-2 Temporal Resolution: Revisit Time

In order to minimize the revisit time, the satellite is configured to have ±45º off-nadir pointing capability. With maximum tilt, the field of regard (FOR) can be extended to more than 600 km from nadir.

The average global revisit time (±45º) is 2 days. See the figure below for more details.

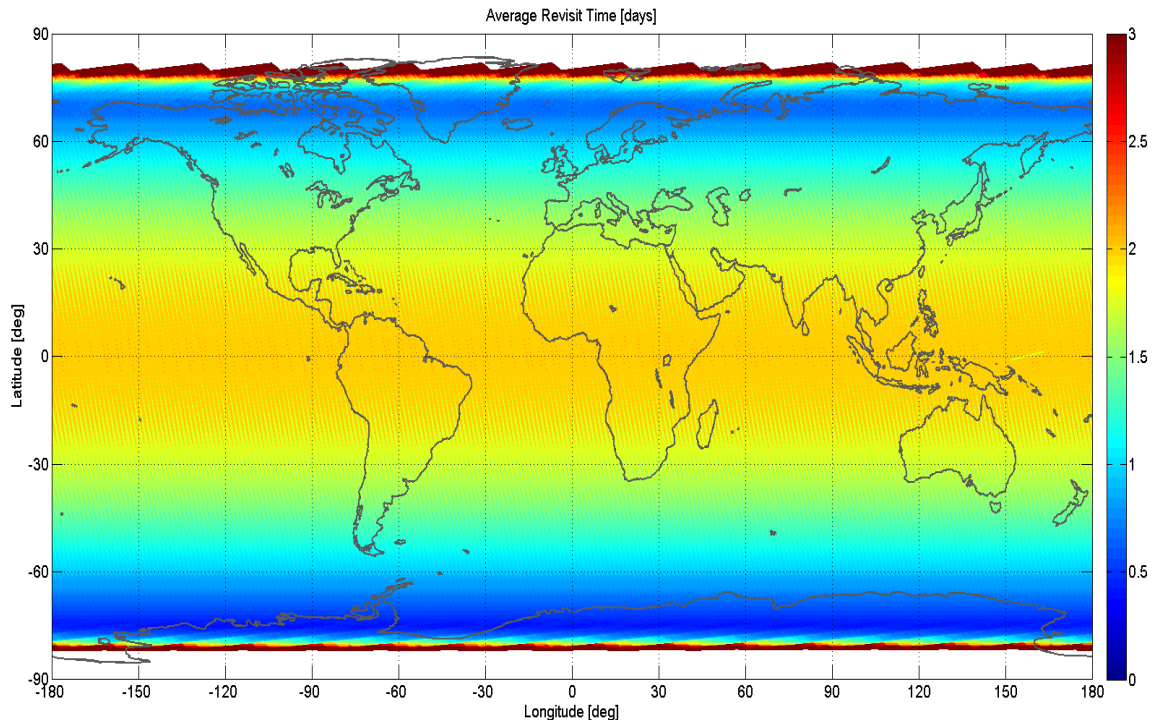Figure 2: DEIMOS-2 Average Revisit Time (days)

Using different maximum observation angles we get different revisit times. The following figures show the influence of the maximum off nadir angle over the maximum and average revisit times.
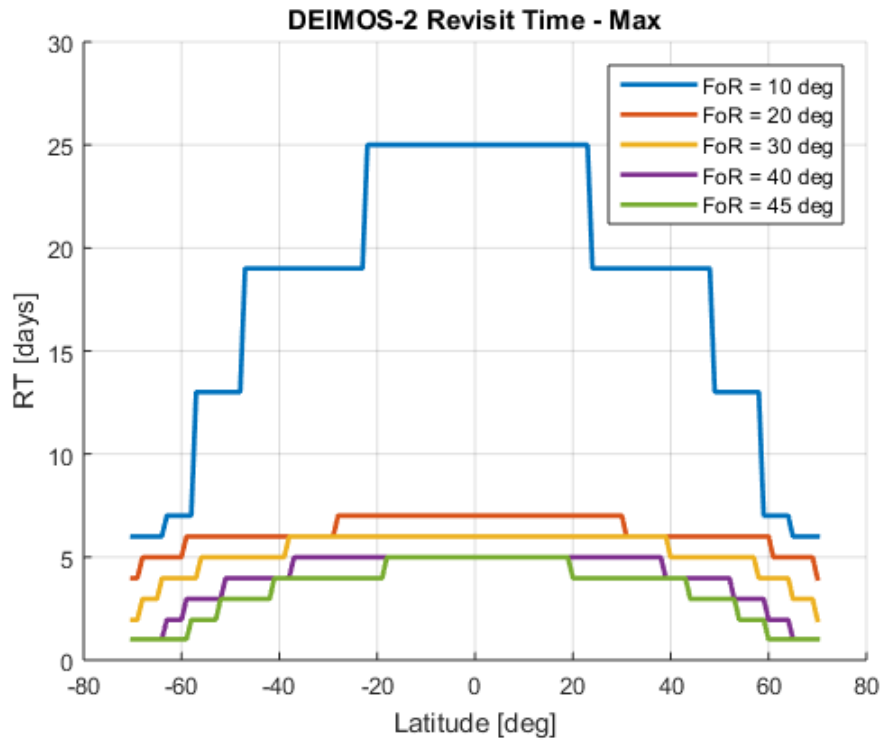
Figure 3: Influence of observation angle and latitude over the maximum revisit time
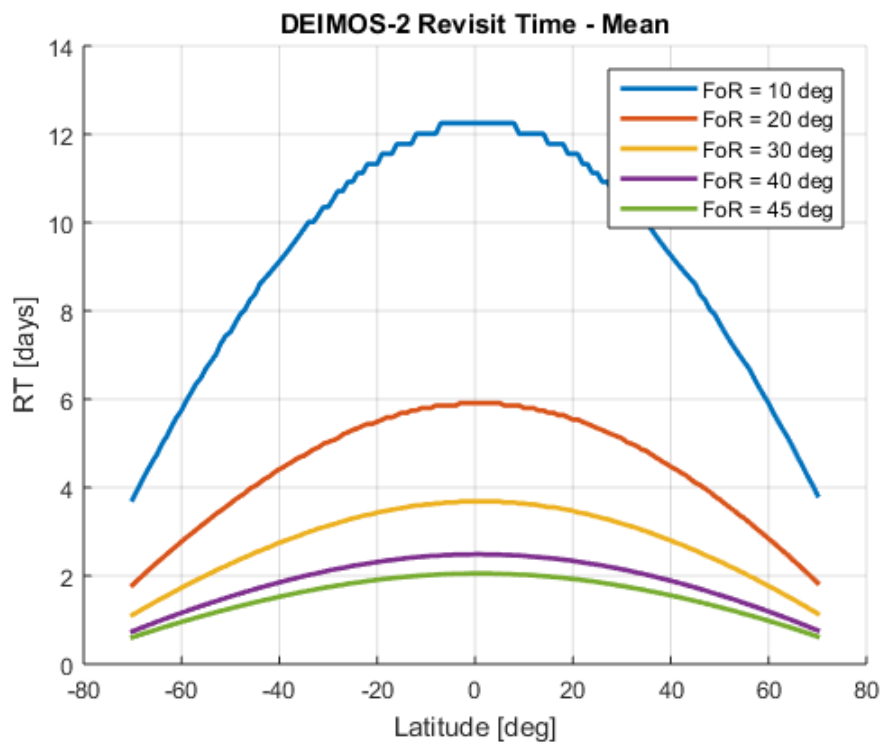
Figure 4: Influence of observation angle and latitude over the mean revisit time

2.2 DEIMOS-2 Ground Sampling Distance

Deimos 2 Ground Sampling Distance is 1 m for PAN band and 4 m for MS bands on nadir conditions. The GSD increases with the observation angle. The following figure shows the influence of the observation angle over the spatial resolution for the PAN band.
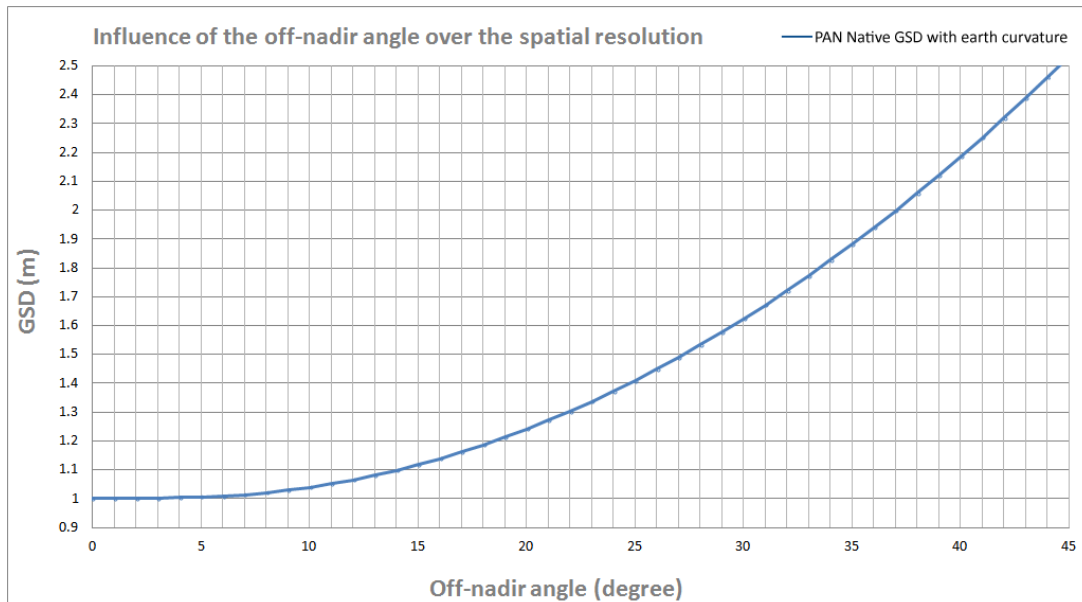
Figure 5: Influence of the off-nadir angle over the spatial resolution

2.3 DEIMOS-2 Processing Levels

DEIMOS-2 products are available in two different processing levels:

Level 1B: A calibrated and radiometrically corrected product, but not resampled. The geometric information is contained in a rational polynomial.

The product includes: the Rational Polynomial Coefficients (RPC); the metadata with gain and bias values for each band, needed to convert the digital numbers into radiances at pixel level, and information about geographic projection (EPGS), corners geolocation, etc.

Level 1C: A calibrated and radiometrically corrected product, manually orthorectified and resampled to a map grid. The geometric information is contained in the GeoTIFF tags.

By default, the reference base for orthorectification is Google Earth. Other user-provided bases can be used on demand.

Typical geometric error of this product (RMSE) is < 20 m. JPEG-2000 format is also available on demand for all processing levels.

The spectral band combination of DEIMOS-2 image products is summarized in the following table.

Product Type	Spectral Bands		
Pan-sharpened	All	R, G, B	NIR, R, G
Pan	Only Pan Band		
MS	Only MS Bands		
Bundle (Pan+MS)	All		

Table 2: Products Characteristics

7

3 Benchmarking Methodology

The results of orthorectification are affected by the quality of the input data and the suitability of the geometric modelling.

The scope of the benchmarking performed during validation of primary products comprises the following components:

- 1 primary image (1B level) with a viewing angle of more than 20 degrees.
- 1 primary image (1B level) with a viewing angle close to nadir.
- The orthocorrection is performed on two independent image processing platforms, ERDAS IMAGINE, PCI Geomatica OrthEngine, providing distinct implementations of RPC models.
- Well defined and highly accurate ancillary data (GCP and DEM).
- Concerning the Ground Control Points used for modelling the orthocorrection process, two different input configurations are used, with three and four GCPs respectively. The same sets are used for both image processing platforms.
- The products are generated using both polynomial orders 0 and 1.
- The ICP used to evaluate the correction performed are as accurate as GCP.

This methodology allows the comparison of the error between different RPC models and orders, using different ancillary data configurations.

In order to fulfil CwRS requirements, the following products are tested:

- Pansharpened products (PSH).
- Panchromatic products (PAN).
- Multispectral products (MS4).

PAN and PSH products share the same geometry, having GSD=1m.
The site used for the tests is located close to Maussane-les-Alpilles, in southern France. It was selected for benchmarking because it offers reference data with a validated quality. It is a rural area with urban settlements which presents an agricultural condition typical for Europe.
PAN and PSH products are validated using one unique set of ICPs estimated over the PAN images.

MS4 products are validated using:
- a 'derived' set of ICPs obtained through a down-sampling of the corresponding PAN ICPs locations;
- a native set of 'located' ICPs directly estimated over the MS4 images.

During the orthorectification process, it was impossible to use the polynomial 1 order to perform orthocorrection with 3 GCPs on ERDAS. In total, **56 products** have been generated and delivered for the test.

	Products	GCP	Model (polynomial order)	ERDAS	PCI	delivered
22,8º viewing angle image	MS	3 (located)	rcp 0 order	1	1	2
		3 (located)	rcp 1 order	0	1	1
		4 (located)	rcp 0 order	1	1	2
		4 (located)	rcp 1 order	1	1	2
		3 (derived)	rcp 0 order	1	1	2
		3 (derived)	rcp 1 order	0	1	1
		4 (derived)	rcp 0 order	1	1	2
		4 (derived)	rcp 1 order	1	1	2
	PSH	3	rcp 0 order	1	1	2
		3	rcp 1 order	0	1	1
		4	rcp 0 order	1	1	2
		4	rcp 1 order	1	1	2
	PAN	3	rcp 0 order	1	1	2
		3	rcp 1 order	0	1	1
		4	rcp 0 order	1	1	2
		4	rcp 1 order	1	1	2
0,8º viewing angle image	MS	3 (located)	rcp 0 order	1	1	2
		3 (located)	rcp 1 order	0	1	1
		4 (located)	rcp 0 order	1	1	2
		4 (located)	rcp 1 order	1	1	2
		3 (derived)	rcp 0 order	1	1	2
		3 (derived)	rcp 1 order	0	1	1
		4 (derived)	rcp 0 order	1	1	2
		4 (derived)	rcp 1 order	1	1	2
	PSH	3	rcp 0 order	1	1	2
		3	rcp 1 order	0	1	1
		4	rcp 0 order	1	1	2
		4	rcp 1 order	1	1	2
	PAN	3	rcp 0 order	1	1	2
		3	rcp 1 order	0	1	1
		4	rcp 0 order	1	1	2
		4	rcp 1 order	1	1	2
TOTAL				24	32	56

Table 3: Description of the generated products

4 Input Imagery

4.1 Selection of AOI over Maussane test site

In order to elaborate the test cases, a set of primary raw images acquired with different viewing angles and a set of well-defined ancillary data (DEM and GCPs) over a well-known area are necessary. The input data used in the benchmarking are presented in this section.

The original AOI is smaller than the area covered by the images. In order to have the control points distributed as evenly as possible, and to control the error over a bigger area, the whole images have been processed. The AOI is located inside both images.

The 15 x 15 km^2 zone acquired by DEIMOS 2 images, which includes the 10 x 10 km^2 AOI, covers an area with agricultural activity, forest, low mountains (300 m) and many urban settlements; with dense coverage by existing CPs datasets.
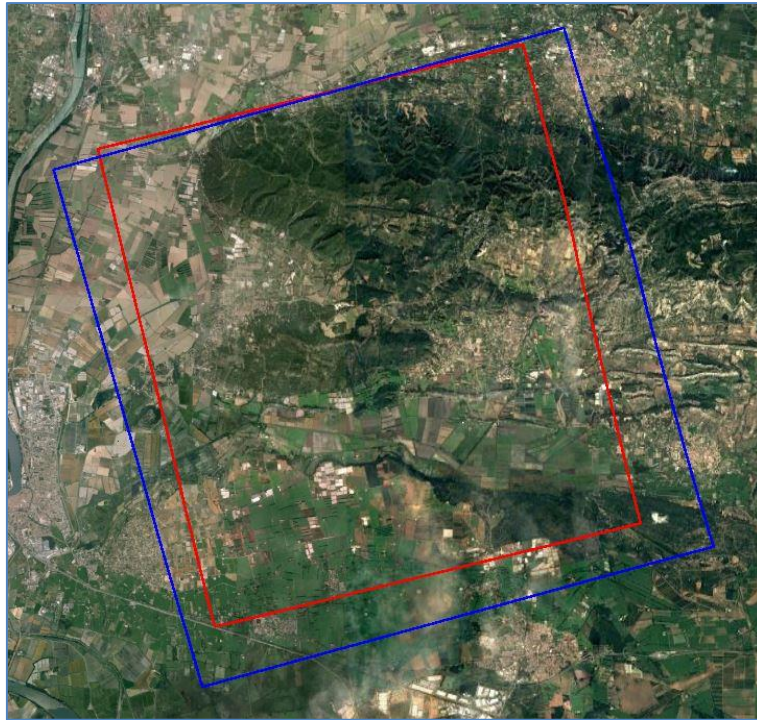
Figure 6: Area covered by the images

4.2 Digital Elevation Model (DEM)

The DEM was obtained from ADS40 project. It was produced from digital airborne stereo pairs. The DEM provided for this process covered all the original AOI, but did not cover all the area acquired by the images. In order to have more GCP available, and to have a better spatial distribution, all the area has been considered.

Where the original DEM was not available, EU-DEM has been used. EU DEM has a pixel size of 25m and a vertical accuracy of +/- 7 m RMSE. All the area where EU-DEM was used is outside the original AOI.

Figure 7: DEM with 0,8º footprint (red); 22,8º footprint (blue) and AOI (green)

4.3 Ground Control Points (GCPs)

Both GCPs and ICPs were retrieved from already existing datasets of differential global positioning system (DGPS) measurements over Maussane test site. These datasets are updated and maintained by JRC.

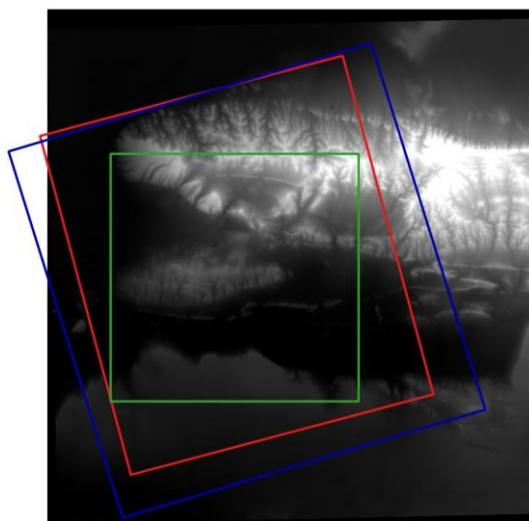Regarding the positional accuracy of ICPs, according to the guidelines, the ICPs should be at least 3 times (5 times recommended) more precise than the target specification, i.e. in our case of a target 5.0 m RMS error the ICPs should have a specification of 1.66 m (1m recommended).

All ICPs that have been selected fulfil therefore the defined criteria. The following table contains the specifications of the used points (Table 4).

Dataset	RMSEx (m)	RMSEy (m)	Number of points
ADS40	0,05	0,10	1
VEXEL	0,49	0,50	6
Cartosat 2	0,90	0,80	2
MAUSS 2009	0,50	0,50	11
MAUSS 2012	0,15	0,15	4
Formosat 2	0,88	0,72	1

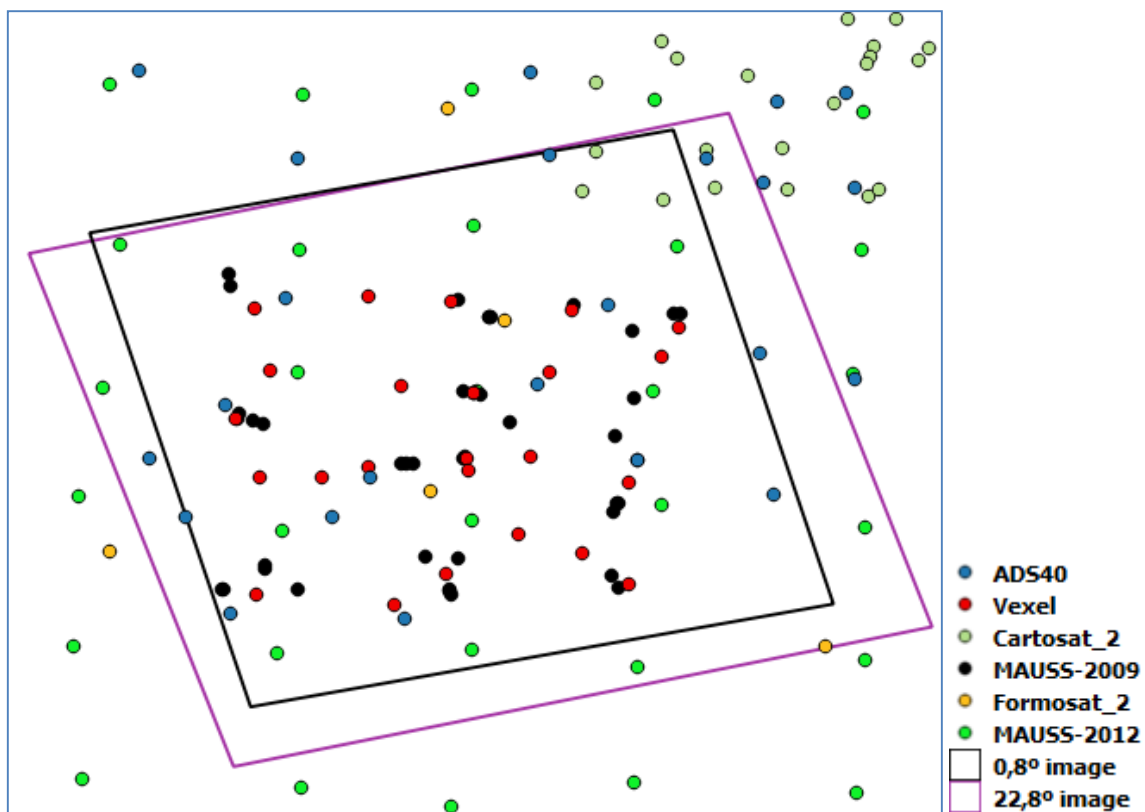Table 4: Control Point Specifications

Figure 8: Available GCPs over the area

4.4 Primary Images

The first image was acquired on the 30th of December 2015, with a viewing angle of around 22,8º. The second image was acquired on the 12th of January 2016, with a viewing angle of 0,8º. These images were used to generate MS4, PAN and PSH products.
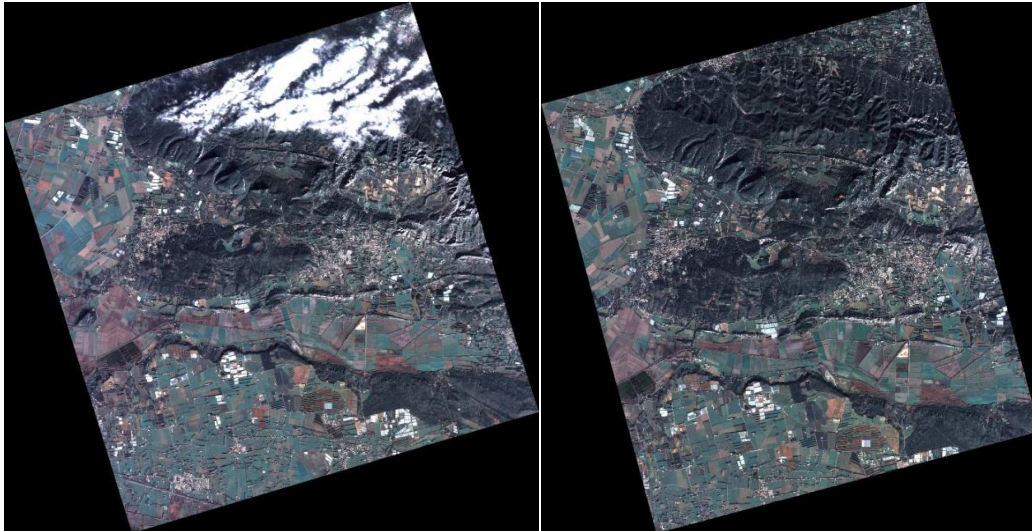

Figure 9: DEIMOS-2 MS4 L1C images with 22,8º (left) and 0,8º (right)

5 Orthorectification

In this validation, it is necessary to use a geometric model, GCPs and DEM to orthorectify images.
Images have a basic RPC model provided by the satellite, which is used together with GCP and DEM in the orthorectification process.
The orthocorrection is performed on two independent image processing platforms, ERDAS IMAGINE, PCI Geomatica OrthEngine, providing distinct implementations of RPC models.

For each image, four GCPs have been selected over the product and they have been used in two different spatialconfigurations, with three and four GCPs. The products have been generated using both polynomial orders 0 and 1 whenever possible. The following image shows the location of the GCPs which were used for the orthorectification of the image with 22,8º viewing angle.

	ID	GCP	
		3	4
1	110008		X
2	110021	X	X
3	440025	X	X
4	66004	X	X

Table 5: GCPs used for 22,8º image
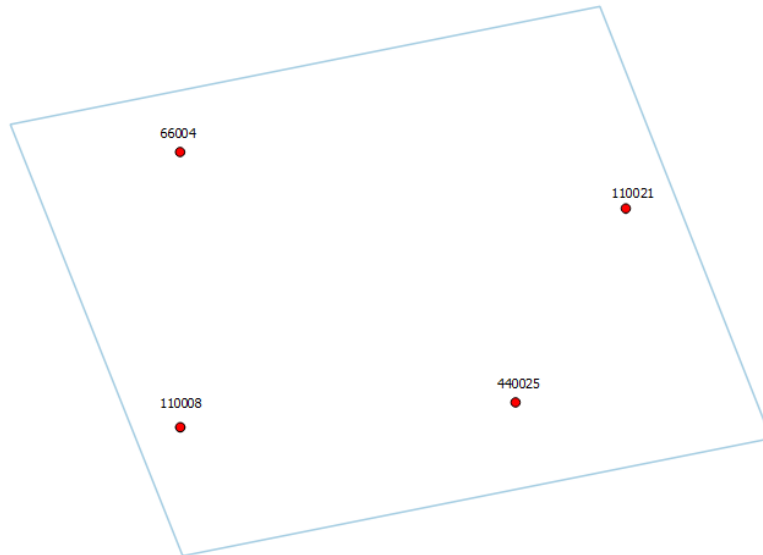
Figure 10: 22,8º footprint and GCPs

The following image shows the location of the GCPs which were used for the orthorectification of the image with 0,8º viewing angle. One of the points used for the orthorectification of the first image was outside the area covered by the second one, so it has been changed for another one.
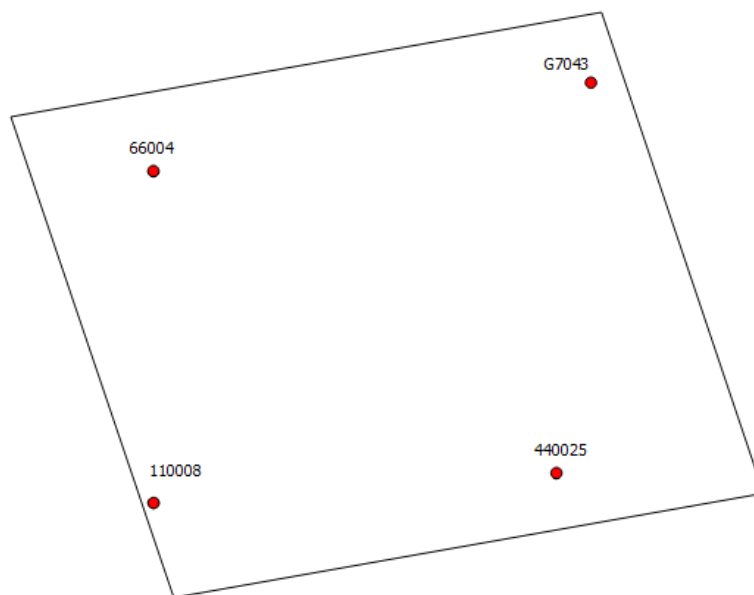
Figure 11: 0,8º footprint and GCPs

		GCP	
	ID	3	4
1	110008	X	X
2	440025	X	X
3	G7043		X
4	66004	X	X

Table 6: GCPs used for 0,8º image

6 External Geometric Quality Control of DEIMOS-2 ortho imagery

6.1 Method for external quality check of ortho images

6.1.1 Independent check points (ICPs) – selection, distribution and registration

The method for the external quality checks (EQCs) strictly follows the Guidelines for Best Practice and Quality Checking of Ortho Imagery [VI].
JRC for the location of ICPs took into account the distribution of the GCPs determined by the FW Contractor which were provided to JRC together with the products. Since the measurements on ICPs have to be completely independent (i.e. ICP must not correspond to GCP used for correction) GCPs taken into account in the geometric correction have been excluded from the datasets considered for EQC.
Both GCPs and ICPs were retrieved from already existing datasets of differential global positioning system (DGPS) measurements over Maussane test site. These datasets are updated and maintained by JRC. Considering the accuracy, distribution and recognisability on the given images, points from 5 datasets were decided to be used for the EQC. The intention was to spread the points evenly across the whole image while keeping at least the minimum recommended number of 20 points [VI].

Due to a low solar angle which caused a lot of shadows, changes of landscape and growing vegetation a JRC operator was not able to keep 20 well distributed point. Therefore for the evaluation of the geometric accuracy of the Deimos-2 ortho imagery, only 17 ICPs for PSH images and 13 ICPs for MSP images were selected.
Because of the low number of ICPs that would be identifiable on Deimos-2 MSP ortho imagery, it was decided to increase for MSP component the number of ICPs by making use of WV3 ortho image. Since the absolute positions (e.g. DGPS measurement) of these check points are not known, the validation results can be interpreted as relative values to the reference ortho image, i.e. WV3 ortho image accuracy. The geometric characteristics of the WV3 image, and in particular its spatial resolution, are significantly better (GSD is 10 times better than the GSD of MSP Deimos-2) than Deimos-2.
Regarding the positional accuracy of ICPs, according to the Guidelines [VI] the ICPs should be at least 3 times more precise than the target specification for the ortho, i.e. in our case of a target 5.0m RMS error (6.0m RMSE for HR profile) the ICPs should have a specification of 1.67m. All ICPs that have been selected fulfil therefore the defined criteria , see Table 8 and Table 8.

The following ortho product was used as reference data:

Sensor	Product	Collection date of the original image	Off nadir angle of the original image	Method used to orthorectify the original image	GSD	Max RMSE of the ortho product
WV3	PSH	8/10/2014	14.1°	RPC, 4GCPs	0.40	0.60

Table 7: Basic metadata of WV3 reference image data used for relative geometric accuracy calculation

Dataset	RMSEx	RMSEy	Number of points
ADS40 GCP_dataset 2003	0,05	0,10	1
VEXEL_GCP_dataset_ 2005	0,49	0,50	6
Multi-use_GCP_dataset_ 2009	0,30	0,30	6
Cartosat-2 dataset 2009	0,90	0,80	2
Campaign 2012 dataset	0,15	0,15	2

Table 8: JRC dataset - Identical check points specifications
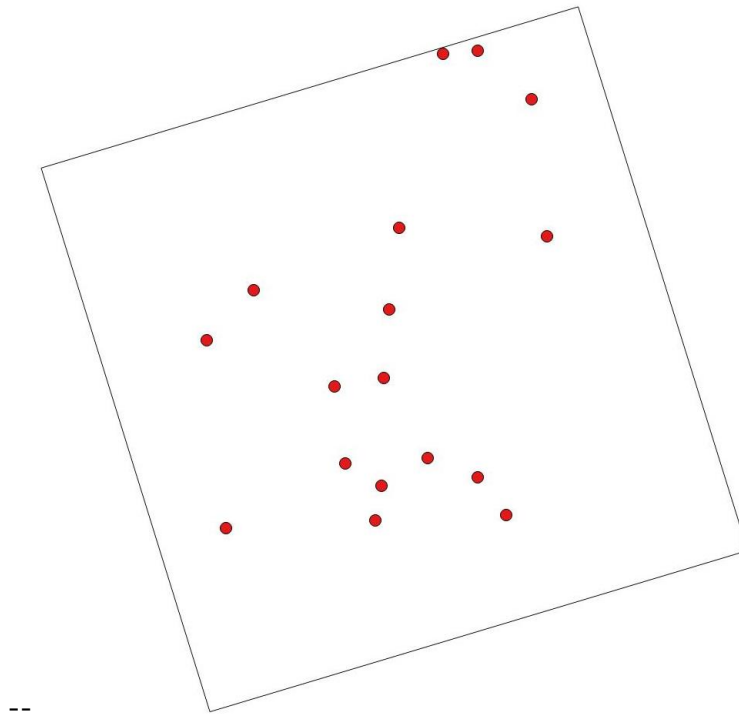
6.1.1.1 ICPs from JRC Dataset

--

Figure 12: ICPs – JRC dataset used by JRC in the EQC of DEIMOS-2 ortho imagery.

ID	E [m]	N [m]
110011	642991,92	4850032,09
G7001	643945,95	4850123,55
G7043	645394,63	4848795,83
66007	641804,02	4845298,88
66024	641320,70	4838276,56
66025	641380,52	4841215,07
66026	640049,05	4840996,07
66035	644717,26	4837489,03
66046	641148,67	4837348,79
440005	645815,17	4845076,11
440008	641527,51	4843087,46

440011	636560,47	4842244,52
440019	642578,11	4839029,46
440021	637082,02	4837127,37
440024	643930,01	4838510,15
C2R4	637829,72	4843609,87
C3R5NEW	640341,36	4838887,55

Table 9: JRC dataset ICPs overview

The projection and datum details of the above mentioned data are UTM 31N zone, WGS 84 ellipsoid.
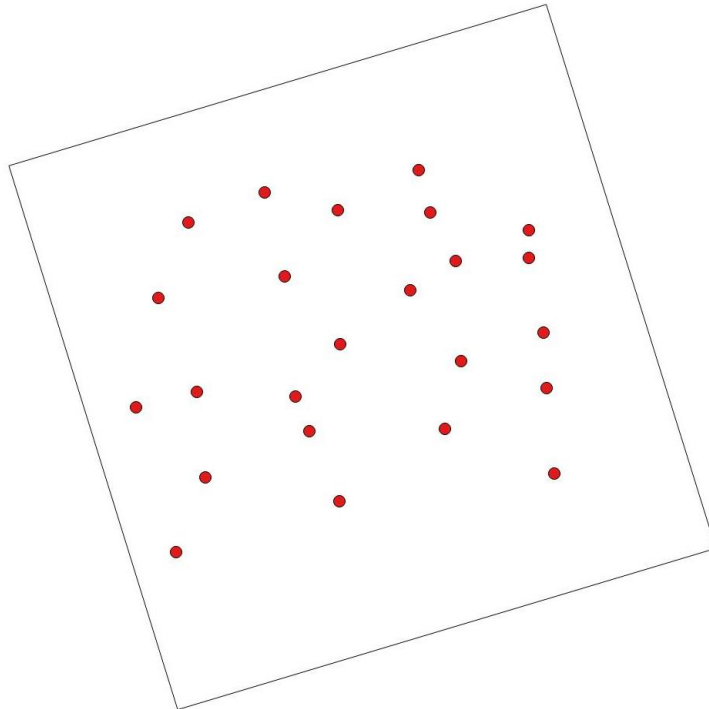
6.1.1.2 ICPs extracted from WV3 image

Figure 13: ICPs – WV3 dataset used by JRC in the EQC of DEIMOS-2 ortho imagery.

ID	E [m]	N [m]
1	636940,92	4845398,08
2	639020,02	4846198,52
3	643198,89	4846804,21
4	641001,54	4845721,65
5	643521,37	4845660,43
6	646205,06	4845173,56
7	646204,33	4844434,36
8	644211,45	4844346,39
9	642981,74	4843545,43
10	639549,14	4843927,94
11	636120,23	4843328,95

12	637164,23	4840783,81
13	639845,34	4840651,27
14	644365,24	4841615,38
15	646606,49	4842388,83
16	646686,11	4840873,24
17	643915,63	4839779,10
18	640227,13	4839716,83
19	635502,96	4840350,39
20	636601,41	4836420,27
21	641050,69	4837807,64
22	646889,41	4838550,81
23	637402,72	4838446,49
24	641070,39	4842074,08

Table 10: WV3 ICPs overview

6.1.2 Computation methodology

Geometric characteristics of orthorectified images are described by Root-Mean-Square Error (RMSE) RMSEx (easting direction) and RMSEy (northing direction) calculated for a set of Independent Check Points.

$$RMSE_{1D}(East) = \sqrt{\frac{1}{n}\sum_{i=1}^{n}\left(X_{REG(i)} - X_{(i)}\right)^2}$$

$$RMSE_{1D}(North) = \sqrt{\frac{1}{n}\sum_{i=1}^{n}\left(Y_{REG(i)} - Y_{(i)}\right)^2}$$

where X,YREG(i) are ortho images derived coordinates, X,Y(i) are the ground true coordinates,   n express the overall number of ICPs used for the validation.

This geometric accuracy representation is called the positional accuracy, also referred to as planimetric/horizontal accuracy and it is therefore based on measuring the residuals between coordinates detected on the orthoimage and the ones measured in the field or on a map of an appropriate accuracy.

All measurements presented in the EQC chapter were carried out in Intergraph ERDAS Imagine 2014 software, using Metric Accuracy Assessment tool for quantitatively measuring the accuracy of an image which is associated with a 3D geometric model. Protocols from the measurements contain other additional indexes like mean errors or error standard deviation that can also eventually help to better describe the spatial variation of errors or to identify potential systematic discrepancies. (Kapnias et al., 2008)[VI].

6.2 Overall results

6.2.1 RMSEs based on ICPs extracted from the JRC Dataset (DGPS measurement)

Off-nadir angle	Number of GCPs	Direction	RMSE [m] 0 RPC order PCI	RMSE [m] 0 RPC order ERDAS	RMSE [m] 1 RPC order PCI	RMSE [m] 1 RPC order ERDAS
0.8°			PAN/PSH			
	3	East	1.72	1.69	1.90	
		North	1.96	1.54	2.13	
	4	East	1.74	2.03	2.07	2.12
		North	1.49	1.88	2.14	1.66
			MSP located			
	3	East	3.32	3.90	3.50	
		North	3.34	3.56	3.15	
	4	East	3.10	3.36	3.09	3.56
		North	3.11	1.77	2.94	2.24
			MSP derived			
	3	East	2.79	3.47	2.93	
		North	3.17	2.98	2.54	
	4	East	2.35	3.39	2.60	3.61
		North	2.44	2.46	2.59	2.31
22.8°			PAN/PSH			
	3	East	1.31	1.98	1.58	
		North	2.77	2.94	2.59	
	4	East	1.35	1.27	1.31	1.18
		North	2.62	2.96	2.64	3.05
			MSP located			
	3	East	3.31	4.24	2.72	
		North	3.40	4.36	3.61	
	4	East	3.38	2.45	2.99	2.69
		North	2.98	2.92	3.14	3.93
			MSP derived			
	3	East	2.93	4.67	2.69	
		North	2.89	4.88	3.16	
	4	East	2.97	2.68	2.93	3.21
		North	3.17	4.11	2.91	3.95

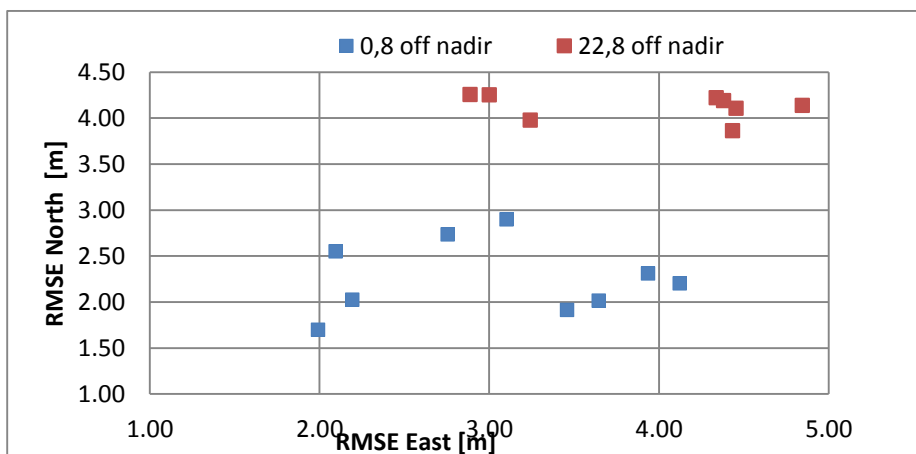Table 11: Results of $RMSE_{1D}$ measurements in JRC ICPs dataset

Figure 14 Point representation of all planimetric RMSE 1D errors measured in the JRC ICPs dataset, distinguished by off nadir angle

Figure 15 Point representation of all planimetric RMSE 1D errors measured in the JRC ICPs dataset, distinguished by a typ of a product

6.2.2 RMSEs based on ICPs extracted from WV3 ortho image

For the additional geometric control of MSP image ortho products was selected only a sample of images, altogether 17 ortho images ware tested with the WV3 dataset.

| Off-nadir angle | Number of GCPs | Direction | RMSE [m] | | | |
| | | | RPC 0 | | RPC 1 | |
			PCI	ERDAS	PCI	ERDAS
0.8°		MSP located				
	3	East	2,75	3,46	n/a	n/a
		North	2,74	1,92	n/a	n/a
	4	East	n/a	n/a	2,10	3,65
		North	n/a	n/a	2,55	2,02
		MSP derived				
	3	East	3,10	4,12	n/a	n/a
		North	2,90	2,20	n/a	n/a
	4	East	2,19	3,93	1,99	n/a
		North	2,03	2,31	1,70	n/a
22.8°		MSP located				
	3	East	2,89	4,34	n/a	n/a
		North	4,26	4,22	n/a	n/a
	4	East	n/a	n/a	4,38	6,04
		North	n/a	n/a	4,19	4,14
		MSP derived				
	3	East	3,00	5,12	n/a	n/a
		North	4,25	4,11	n/a	n/a
	4	East	3,24	n/a	4,43	n/a
		North	3,98	n/a	3,86	n/a

Table 12: Results of RMSE 1D measurements in the WV3 ICPs dataset on MSP image

Figure 16 Point representation of planimetric RMSE 1D errors measured in the WV3 ICPs dataset on MSP image, distinguished by off nadir angle
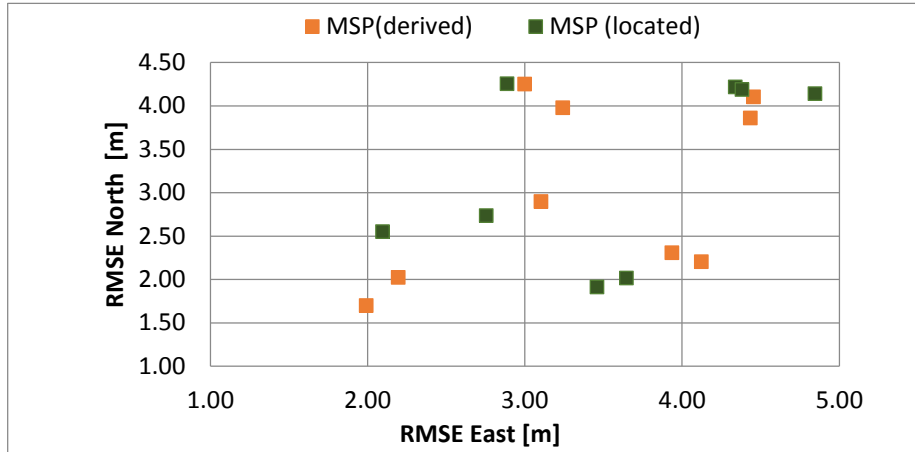
Figure 17 Point representation of all planimetric RMSE1D errors measured in the WV3 ICPs dataset, distinguished by a typ of a product
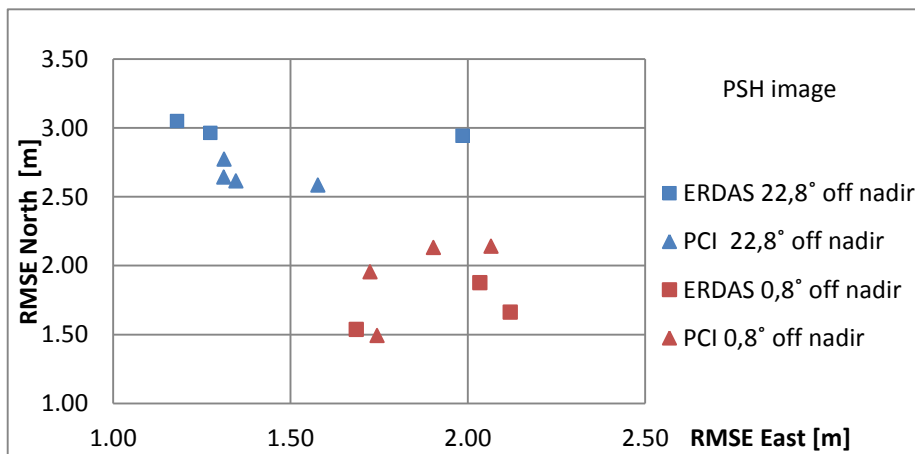
6.3 Discussion on off-nadir angle factor

Figure 18 Point representation of planimetric RMSE1D errors measured in the JRC ICPs dataset on PSH ortho products, distinguished acording to the off nadir angle and software
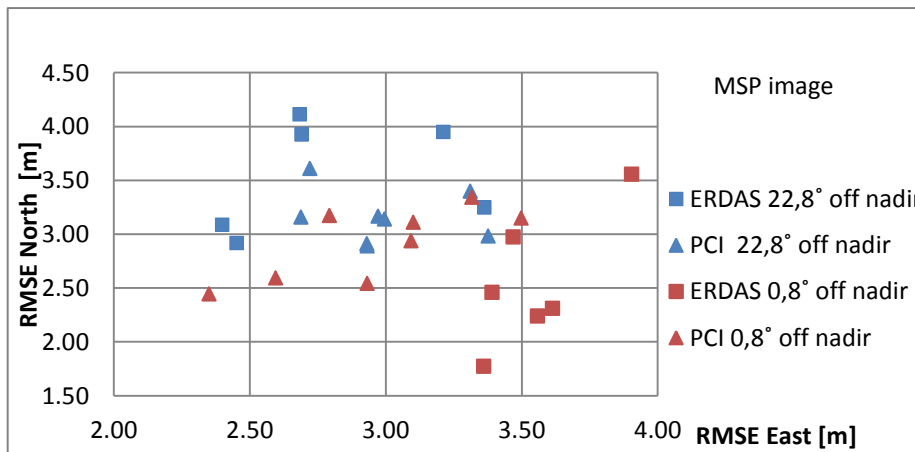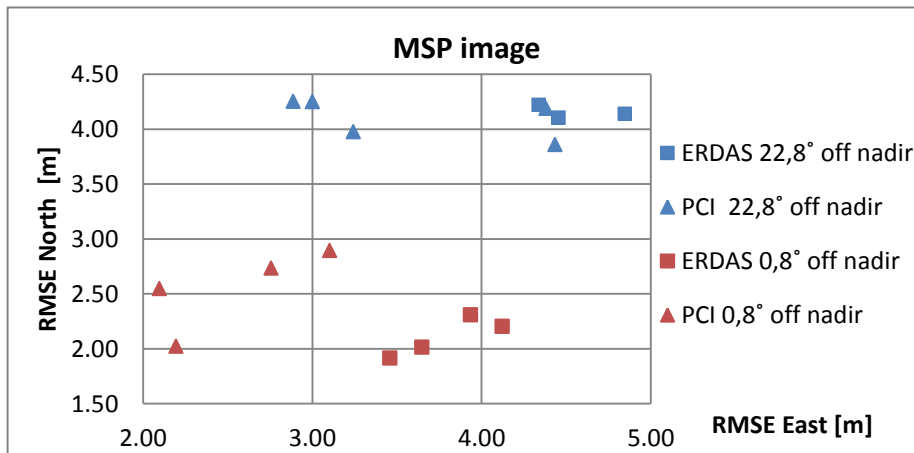
Figure 19 Point representation of planimetric RMSE1D errors measured in the JRC ICPs dataset on MSP ortho products, distinguished acording to the off nadir angle and software

Figure 20 Point representation of planimetric RMSE1D errors measured in the WV3 ICPs dataset on MSP ortho products, distinguished acording to the off nadir angle and software

Comparing the results displayed in the Figures 14-20 (additional charts in the Annex 2: Figure 24, Figure 25, Figure 26), we can summarize the following findings:

- The RMSEs in the Northing direction are sensitive to the overall off nadir angle of the acquired scene. The increase with the increasing off nadir angle is observed.

- The RMSEs in the Easting direction behave differently for the JRC dataset of ICPs and the WV3 dataset.

- While for the JRC dataset the RMSEs in the Easting direction paradoxically decrease with the increasing off nadir angle (especially for the PSH product), the RMSEs measured on WV3 ICPs dataset with the increasing off nadir angle seem to get worse.

6.4 Discussion on the number and distribution of GCPs used for the modelling

6.4.1 Number of GCPs

Looking at charts in the Annex 2(Figure 27) we can conclude there is no clear evidence that changing a number of GCPs from 3 to 4 would have an impact on the geometric accuracy of the final ortho product.

6.4.2 Distribution of GCPs

The geometric accuracy of the ortho image depends on (except others) the accuracy of the input orientation parameters, i.e also on the distribution of ground control points over the model.

Some RMSEs of ortho products derived using 22.8 off nadir angle image are close to the threshold. To understand better why these image products (i.e. 22.8 off nadir) give worse RMSEs, we studied more in detail all measured residuals on ICPs. It resulted that there are ICPs laying in a hilly area, giving always huge residuals (10m-15m), which have a strong influence on the final RMSE.

From the figure 9 and figure10 could be seen that a classical distribution of GCPs (for instance figure 11) was impossible to use due to the fit cloud cover in the upper right corner of the image. This part of the image contains also a mountainous range. Unavailability of visible GCPs in this hilly area and subsequently their not correct distribution caused large geometrical errors at certain parts of the ortho image.

6.5 Discussion on software usage factor

To compare algorithms implemented in different COTS, ERDAS IMAGINE 2016 and PCI Geomatica 2016 software were selected to derive the corresponding ortho products from the acquired image scenes.

From the Figures 18-20 (or see also other charts in Annex 2: Figure 28, Figure 29, Figure 30) could be concluded following:

- As far as the JRC ICPs database is concerned, the performance of both software packages is very similar.
- The values measured on the WV3 ICPs dataset differ according to the axis direction. The ortho images produced by PCI have apparently lower RMSEs in the Easting direction. For the Northing direction the RMSEs values are more or less equal.

6.6 Discussion on RPC order used for modelling

Looking at charts in Annex 2: Figure 31, we can summarize that there is no clear evidence that one RPC order would perform generally better than the other one.

6.7 Discussion on the nature of GCPs

As mentioned in the chapter 3 Benchmarking methodology MSP products were generated using so-called 'derived' and 'located' GCPs.

This analysis should help in decision whether full exploitation of the spatial information available in the PAN image(part of the bundle product) helps to improve the overall geometric quality of the final ortho product.
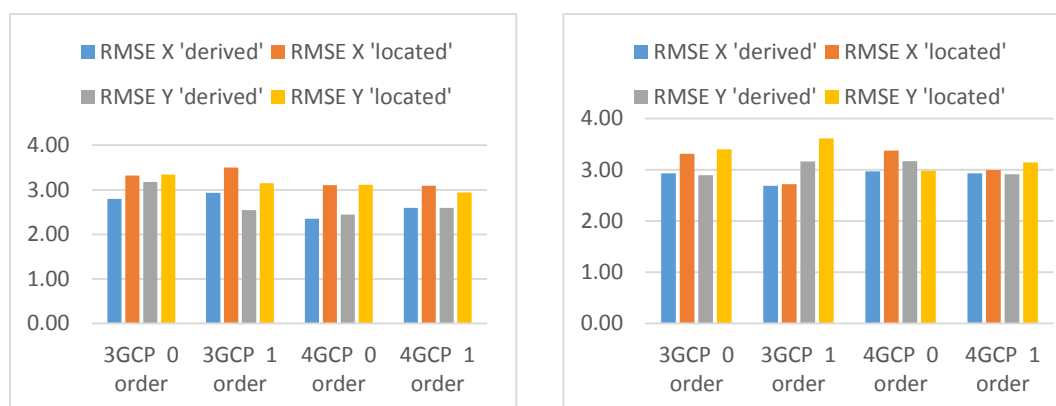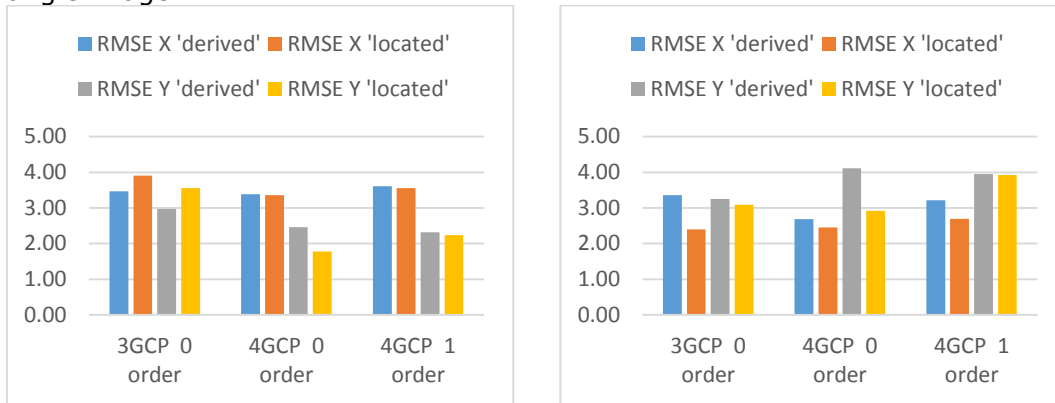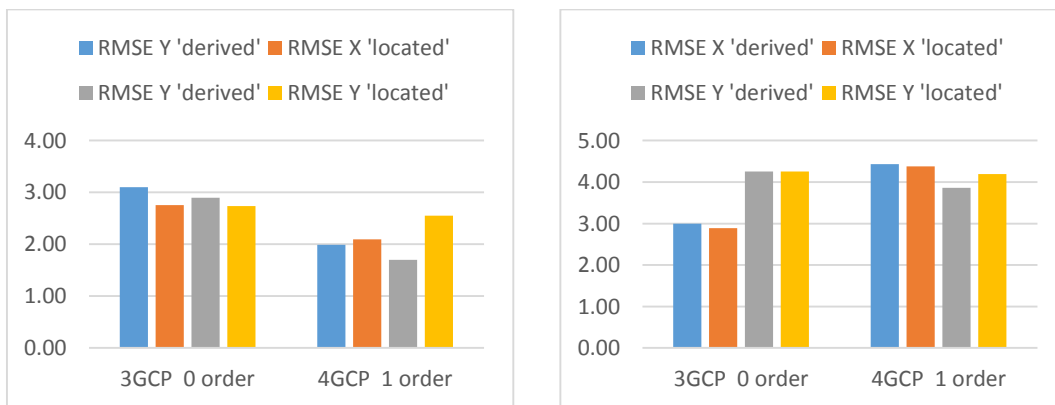

Figure 21 Graph representation of RMSEs comparison between orthoimages produced using "located" and "derived" GCPs

RMSEs measured in the **JRC ICPs dataset**, on MSP images produced by **PCI Geomatics** software. From left to right: 0.8˚ off nadi angle image , 22.8˚ off nadir angle image

Figure 22 Graph representation of RMSEs comparison between orthoimages produced using "located" and "derived" GCPs

RMSEs measured in the **JRC ICPs dataset**, on MSP images produced by **ERDAS Imagine** software. From left to right: 0.8˚ off nadi angle image , 22.8˚ off nadir angle image

Figure 23 Graph representation of RMSEs comparison between orthoimages produced using "located" and "derived" GCPs

RMSEs measured in the **WV3 ICPs dataset**, on MSP images produced by **PCI Geomatics** software. From left to right: 0.8˚ off nadi angle image , 22.8˚ off nadir angle image

Looking at results displayed in the Figure 21, Figure 22, Figure 23 we can conclude that:
- There is the no clear evidence that applying "derived" GCPs during the modelling phase results in a better positional accuracy (i.e. lower RMSEs) of the final ortho products

7 Conclusion

Following the findings presented in this report it is asserted that:

- The Deimos-2 MSP orthoimagery geometric accuracy meets the requirement of 1.5xGSDm 1D RMSE (GSD≤25m) corresponding to the F0.HR prime CwRS profile defined in the HR profile based technical specifications, on condition that RPC model and at least 3 GCPs are applied to generate the ortho product.

- The Deimos-2 MSP orthoimagery geometric accuracy meets the requirement of 5m 1D RMSE (GSD≤12m) corresponding to the F1.HHR prime CwRS profile defined in the HR profile based technical specifications, on condition that RPC model and at least 3 GCPs are applied to generate the ortho product.

- The Deimos-2 PAN/PSH orthoimagery geometric accuracy meets the requirement of 5m 1D RMSE (GSD≤3m) corresponding to the F1.HHR prime CwRS profile defined in the HR profile based technical specifications, on condition that RPC model and at least 3 GCPs are applied to generate the ortho product.

- The Deimos-2 PAN/PSH orthoimagery geometric accuracy meets the requirement of 5m 1D RMSE (GSD≤3m) corresponding to the E. VHR backup profile defined in the VHR profile based technical specifications, on condition that RPC model and at least 3 GCPs are applied to generate the ortho product.

As regards the factors influencing the final orthoimage accuracy, following general conclusions can be drawn:

- With respect to CAP checks purposes, both software packages (PCI Geomatics and ERDAS Imagine) suite for the orthoimage generation.

- The tested ortho products fulfil the CAP requirements as soon as at least 3 GCPs are applied. The increasing number of GCPs does not have any substantial effect on the positional accuracy of ortho products. However, where possible, it is suggested to use 4 GCPs.

- There is no clear evidence that the exploitation of a high resolution PAN band to localise a position of GCPs on a MSP image improves the final geometric accuracy of the product. However it is recommended to fully benefit from the high-resolution spatial information of bundle (PAN+MSP) products and use "derived" GCPs

- It appears that there is not a big difference between a zero RPC order transformation and an affine transformation when orthoreftifying Deimos-2 images. The decision on which polynomial order use for the refinement very depends on the number of GCPs available, their quality,distribution over the whole scene and software available.

- An attention should be paid to the well distribution of GCPs over an image, especially when orthorectifying hilly areas.
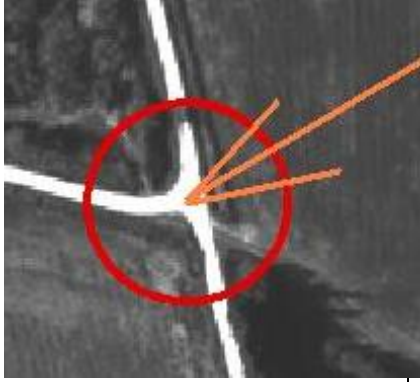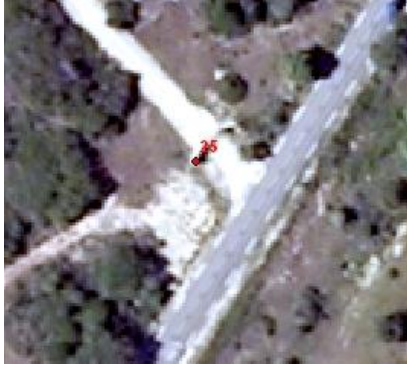
ANNEX 1 Description of GCPs

Some information regarding the GCPs used for orthorectification process is provided here.

22,8º		In-situ measured GPS (North, East) coordinates in EPSG 32631 reference system and respective heights			PAN		MS derived		MS located	
	GCP	Reference x	Reference y	Elevation_m	column	row	column	row	column	row
1	110008	636561,549	4836585,549	30,296	934,9	9476,6	233,725	2369,15	233,875	2368,625
2	110021	647527,989	4844367,306	115,567	10718,9	5825,9	2679,725	1456,475	2679,625	1456,625
3	440025	644920,321	4837617,876	5,307	7290,6	10665,4	1822,65	2666,35	1822,375	2666,625
4	66004	636363,62	4846077,515	5	2952,4	1747,9	738,1	436,975	737,875	436,625

Table 13: selected GCPs for 22,8º image.

0,8º		In-situ measured GPS (North, East) coordinates in EPSG 32631 reference system and respective heights			PAN		MS derived		MS located	
	GCP	Reference x	Reference y	Elevation_m	column	row	column	row	column	row
1	110008	636561,549	4836585,549	30,296	225,875	10569,875	56,46875	2642,46875	56,264	2642,128
2	440025	644920,321	4837617,876	5,307	7968,875	11635,125	1992,21875	2908,78125	1992,375	2908,375
3	G7043	645394,626	4848795,83	34,639	11068,875	1763,125	2767,21875	440,78125	2767,317	440,112
4	66004	636363,62	4846077,515	5	2327,375	2043,625	581,84375	510,90625	581,427	510,374

Table 14: selected GCPs for 0,8º image.

ID	source	Location	Ground camera shots
66004	MAUSS 2009		
44025	VEXEL 2005		
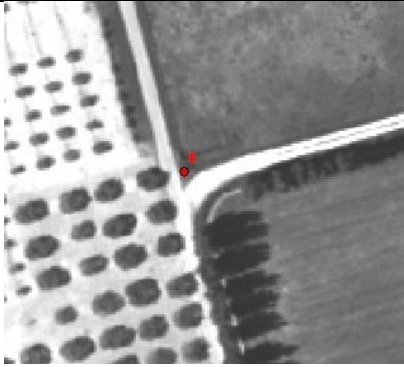
ID	source	Location	Ground camera shots
110008	ASD40 2003		
110021	ASD40 2003		
G7043	CARTOSAT2 2009		

Table 15 GCPs selection over Maussane site – screen-shots and camera-shots

ANNEX 2 Internal Geometric Quality Control

The following tables show the control point residuals obtained during the orthorectification process:

0,8º IMAGE							
ERDAS				**PCI**			
PAN				**PAN**			
ORDER 0	Control point residuals (m)			ORDER 0	Control point residuals (m)		
Point	rX	rY	rZ	Point	rX	rY	rZ
1	-0,5513	0,9335	0,0002	1	-0,530	1,017	
2	0,8948	0,2404	-0,0005	2	0,855	0,320	
3	-0,6635	-0,3790	0,0003	3	-0,692	-0,473	
4	0,3207	-0,7949	-0,0002	4	0,367	-0,866	
ORDER 0	Control point residuals (m)			ORDER 0	Control point residuals (m)		
Point	rX	rY	rZ	Point	rX	rY	rZ
1	-0,7727	0,8073	0,0004	1	-0,797	0,811	
2	0,6730	0,1137	-0,0004	2	0,588	0,113	
4	0,0991	-0,9213	-0,0001	4	0,101	-1,073	
ORDER 1	Control point residuals (m)			ORDER 1	Control point residuals (m)		
Point	rX	rY	rZ	Point	rX	rY	rZ
1	-0,6613	0,3575	0,0004	1	-0,602	0,688	
2	0,5721	-0,3096	-0,0003	2	0,749	0,063	
3	-0,5279	0,2859	0,0003	3	-0,608	-0,095	
4	0,6171	-0,3338	-0,0004	4	0,46	-0,658	
				ORDER 1	Control point residuals (m)		
				Point	rX	rY	rZ
				1	-0,656	0,633	
				2	0,475	0,007	
				4	0,070	-0,824	

Table 16: 0,8º PAN GCP residuals

0,8º IMAGE							
ERDAS				**PCI**			
MS Derived				**MS Derived**			
ORDER 0	Control point residuals (m)			ORDER 0	Control point residuals (m)		
Point	rX	rY	rZ	Point	rX	rY	rZ
1	-0,5123	0,8675	0,0002	1	-0,530	1,018	
2	0,8318	0,2235	-0,0005	2	0,855	0,321	
3	-0,6168	-0,3523	0,0003	3	-0,692	-0,473	
4	0,2979	-0,7387	-0,0002	4	0,367	-0,866	
ORDER 0	Control point residuals (m)			ORDER 0	Control point residuals (m)		
Point	rX	rY	rZ	Point	rX	rY	rZ
1	-0,7182	0,7502	0,0004	1	-0,760	0,861	
2	0,6257	0,1058	-0,0003	2	0,624	0,163	
4	0,0919	-0,8562	-0,0001	4	0,137	-1,023	
ORDER 1	Control point residuals (m)			ORDER 1	Control point residuals (m)		
Point	rX	rY	rZ	Point	rX	rY	rZ
1	-0,6147	0,3322	0,0003	1	-0,557	0,897	
2	0,5319	-0,2876	-0,0003	2	0,820	0,234	
3	-0,4908	0,2656	0,0003	3	-0,661	-0,334	
4	0,5737	-0,3101	-0,0004	4	0,398	-0,796	
				ORDER 1	Control point residuals (m)		
				Point	rX	rY	rZ
				1	-0,725	0,812	
				2	0,584	0,114	
				4	0,141	-0,926	

Table 17: 0,8º MS Derived GCP residuals

0,8º IMAGE							
ERDAS				PCI			
MS Located				MS Located			
ORDER 0	Control point residuals (m)			ORDER 0	Control point residuals (m)		
Point	rX	rY	rZ	Point	rX	rY	rZ
1	-0,7992	0,1858	0,0005	1	-0,837	0,281	
2	1,8701	0,1645	-0,001	2	1,979	0,258	
3	-0,0723	0,5461	0,0001	3	-0,104	0,500	
4	-10014	-0,8974	0,0006	4	-1,037	-1,037	
ORDER 0	Control point residuals (m)			ORDER 0	Control point residuals (m)		
Point	rX	rY	rZ	Point	rX	rY	rZ
1	-0,8231	0,3679	0,0005	1	-0,872	0,448	
3	1,8462	0,3466	-0,001	2	1,944	0,425	
4	-1,0253	-0,7153	0,0006	4	-1,072	-0,870	
ORDER 1	Control point residuals (m)			ORDER 1	Control point residuals (m)		
Point	rX	rY	rZ	Point	rX	rY	rZ
1	-0,4727	0,4045	0,0002	1	-0,810	0,296	
2	0,4092	-0,3502	-0,0002	2	1,811	0,189	
3	-0,3776	0,3233	0,0002	3	-0,128	0,486	
4	0,4412	-0,3776	-0,0003	4	-0,873	-0,969	
				ORDER 1	Control point residuals (m)		
				Point	rX	rY	rZ
				1	-0,842	0,419	
				2	1,765	0,363	
				4	-0,922	-0,780	

Table 18: 0,8º MS Located GCP residuals

22,8º IMAGE							
ERDAS				PCI			
PAN				PAN			
ORDER 0	Control point residuals (m)			ORDER 0	Control point residuals (m)		
Point	rX	rY	rZ	Point	rX	rY	rZ
1	-0,7595	-0,8529	0,3428	1	1,209	-0,955	
2	-0,6230	-0,3064	0,2687	2	1,622	-0,389	
3	0,9064	1,3669	-0,4173	3	3,568	1,618	
4	0,4792	-0,2069	-0,1967	4	3,021	-0,378	
ORDER 0	Control point residuals (m)			ORDER 0	Control point residuals (m)		
Point	rX	rY	rZ	Point	rX	rY	rZ
1	-0,8779	-0,5910	0,3827	2	2,697	-0,636	
2	0,6506	1,0821	-0,3023	3	4,647	1,373	
4	0,2223	-0,4928	-0,0815	4	4,108	-0,621	
ORDER 1	Control point residuals (m)			ORDER 1	Control point residuals (m)		
Point	rX	rY	rZ	Point	rX	rY	rZ
1	-0,6845	-0,6706	0,3063	1	1,241	-0,949	
2	-0,6955	-0,6736	0,3084	2	1,269	-0,429	
3	0,9159	0,8903	-0,4082	3	2,977	1,552	
4	0,4637	0,4536	-0,2064	4	3,707	-0,298	
				ORDER 1	Control point residuals (m)		
				Point	rX	rY	rZ
				2	0,401	-0,669	
				3	1,936	0,986	
				4	6,298	-0,386	

Table 19: 22,8º PAN GCP residuals

22,8º IMAGE

ERDAS MS Derived				PCI MS Derived			
ORDER 0 Point	Control point residuals (m) rX	rY	rZ	ORDER 0 Point	Control point residuals (m) rX	rY	rZ
1	-0,2443	-0,2781	0,1104	1	-1,160	-0,933	
2	-0,2064	-0,0982	0,0890	2	-0,717	-0,358	
3	0,2925	0,4491	-0,1349	3	1,219	1,646	
4	0,1592	-0,0727	-0,0653	4	0,658	-0,355	
ORDER 0 Point	Control point residuals (m) rX	rY	rZ	ORDER 0 Point	Control point residuals (m) rX	rY	rZ
1	-0,2890	-0,1912	0,1259	2	-1,098	-0,667	
2	0,2102	0,3562	-0,0978	3	0,835	1,336	
4	0,0772	-0,1656	-0,0284	4	0,272	-0,667	
ORDER 1 Point	Control point residuals (m) rX	rY	rZ	ORDER 1 Point	Control point residuals (m) rX	rY	rZ
1	-0,2228	-0,2185	0,0997	1	-1,138	-0,909	
2	-0,2264	-0,2195	0,1004	2	-0,739	-0,406	
3	0,2981	0,2901	-0,1329	3	1,219	1,581	
4	0,1509	0,1478	-0,0672	4	0,659	-0,266	
				ORDER 1 Point	Control point residuals (m) rX	rY	rZ
				2	-1,059	-0,664	
				3	0,810	1,253	
				4	0,258	-0,587	

Table 20: 22,8º MS Derived GCP residuals

22,8º IMAGE

ERDAS MS Located				PCI MS Located			
ORDER 0 Point	Control point residuals (m) rX	rY	rZ	ORDER 0 Point	Control point residuals (m) rX	rY	rZ
1	-0,0882	0,3797	0,0267	1	-0,420	1,326	
2	-0,0858	-0,4422	0,0472	2	-0,286	-1,526	
3	0,2353	-0,1318	-0,0950	3	0,953	-0,349	
4	-0,0626	0,1939	0,0216	4	-0,241	0,549	
ORDER 0 Point	Control point residuals (m) rX	rY	rZ	ORDER 0 Point	Control point residuals (m) rX	rY	rZ
1	-0,1151	-0,3156	0,0563	2	-0,427	-1,084	
3	0,2060	-0,0052	-0,0862	3	0,813	0,093	
4	-0,0920	0,3204	0,0309	4	-0,381	0,991	
ORDER 1 Point	Control point residuals (m) rX	rY	rZ	ORDER 1 Point	Control point residuals (m) rX	rY	rZ
1	-0,1044	-0,0041	0,044	1	-0,418	1,183	
2	-0,1056	-0,0045	0,0443	2	-0,304	-1,365	
3	0,1393	0,0058	-0,0585	3	0,915	-0,301	
4	0,0707	0,0029	-0,0298	4	-0,187	0,483	
				ORDER 1 Point	Control point residuals (m) rX	rY	rZ
				2	-0,424	-1,027	
				3	0,764	0,128	
				4	-0,335	0,900	

Table 21: 22,8º MS Located GCP residual

ANNEX 3 Supporting charts to the ECQ of JRC

See the chapter 6.3 Discussion on off-nadir angle factor
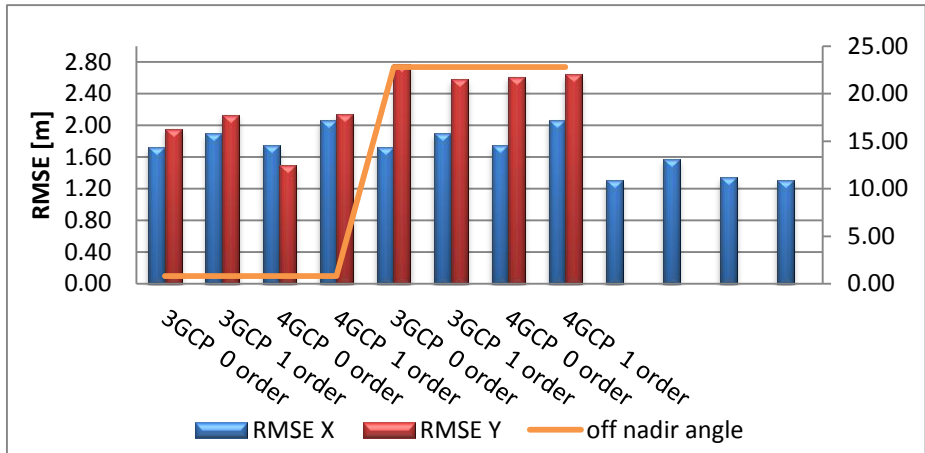
Figure 24 Graph of RMSEs as a function of the number of GCPs + the RPC order and off nadir angle measured over PSH ortho images
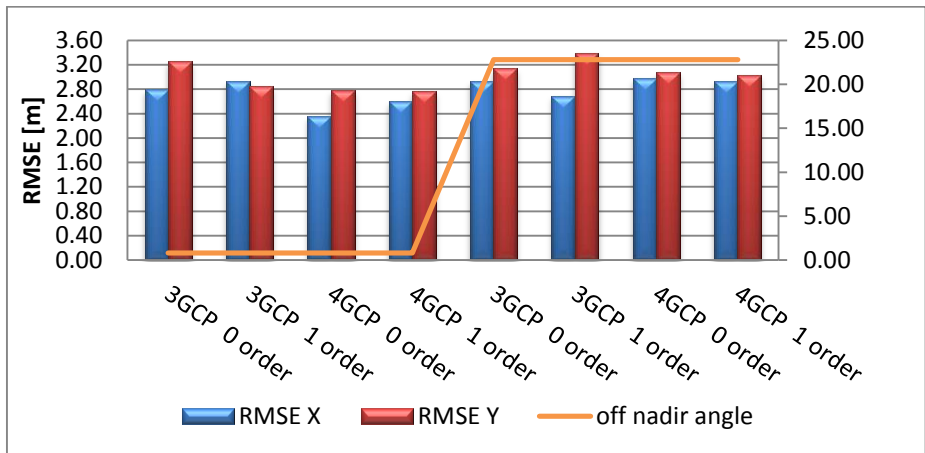
Figure 25 Graph of average RMSEs as a function of the number of GCPs + the RPC order and off nadir angle, calculated for MSP(derived) and MSP (located) ortho products in the JRC dataset (PCI software)
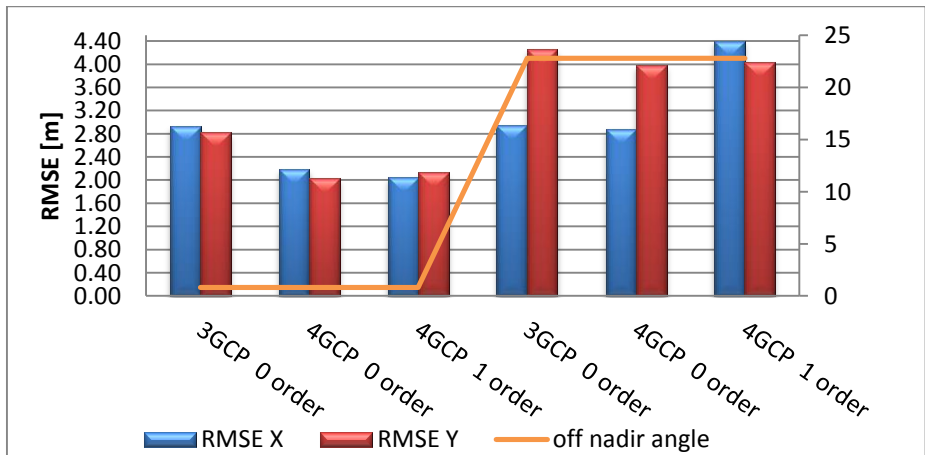
Figure 26 Graph of average RMSEs as a function of the number of GCPs + the RPC order and off nadir angle, calculated for MSP(derived) and MSP (located) ortho products in the WV3 dataset (PCI software)

See the chapter 6.4Discussion on the number and distribution of GCPs used for the modelling
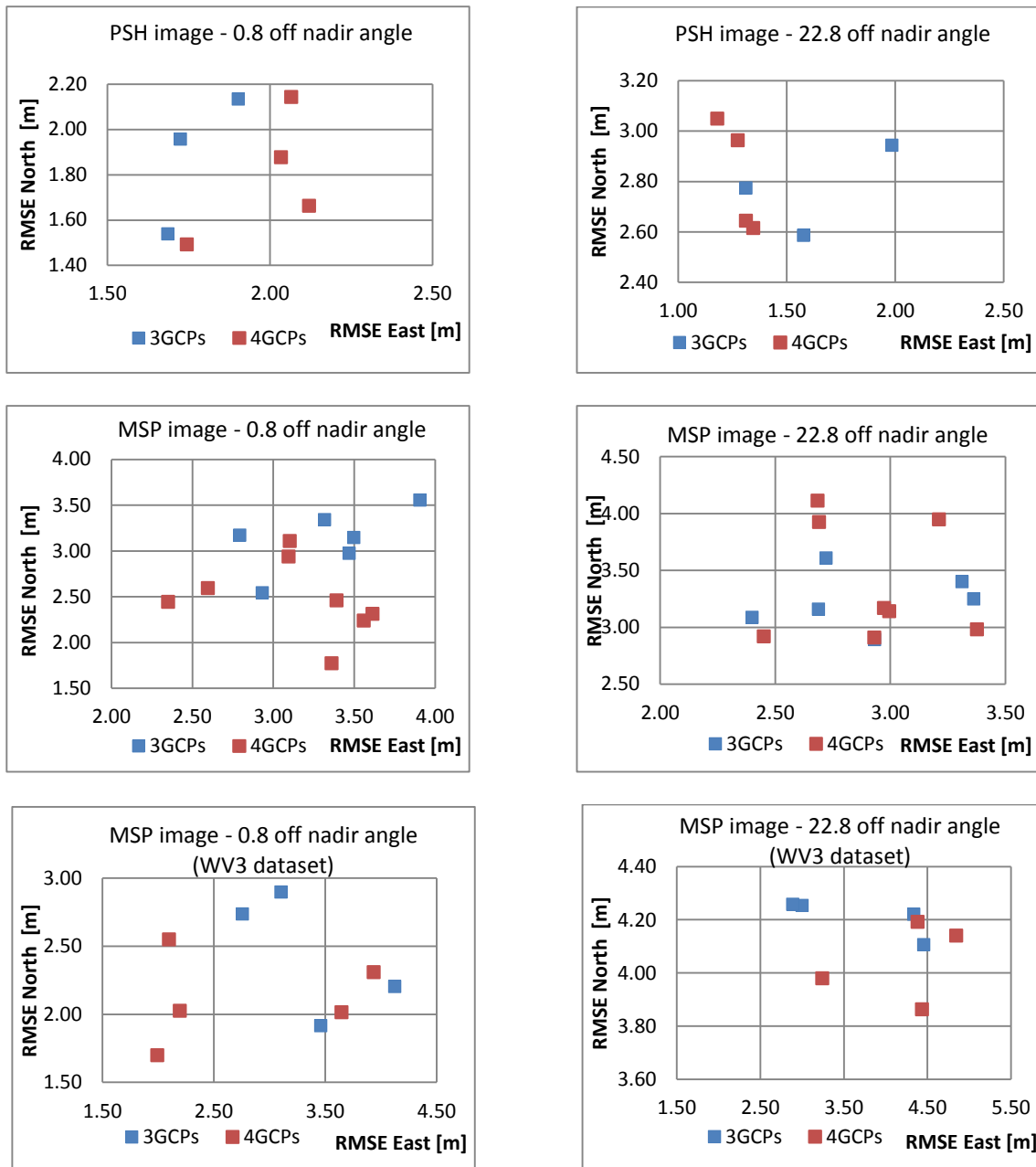
Figure 27 Point representation of planimetric RMSE1D errors measured ortho products, distinguished acording to the number of GCPs

See the chapter 6.5Discussion on software usage factor
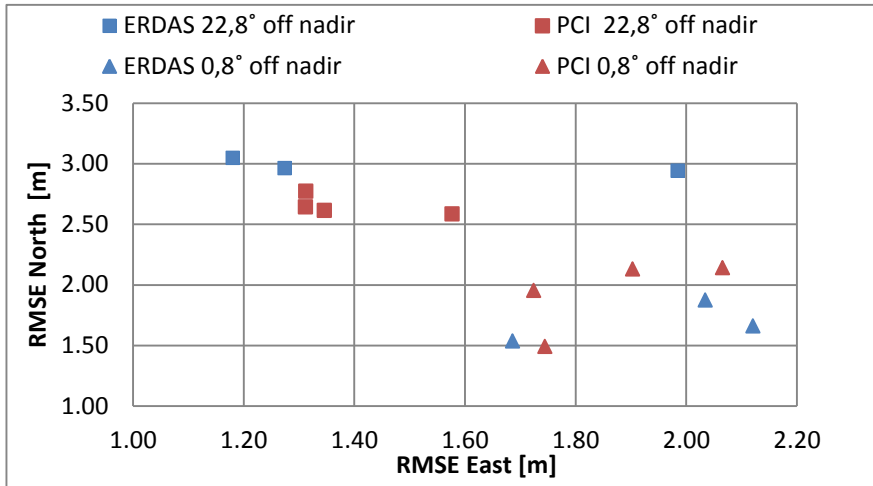
Figure 28 Point representation of planimetric RMSE1D errors measured in the JRC dataset on PSH ortho products, distinguished acording to the off nadir angle and the sofware used.
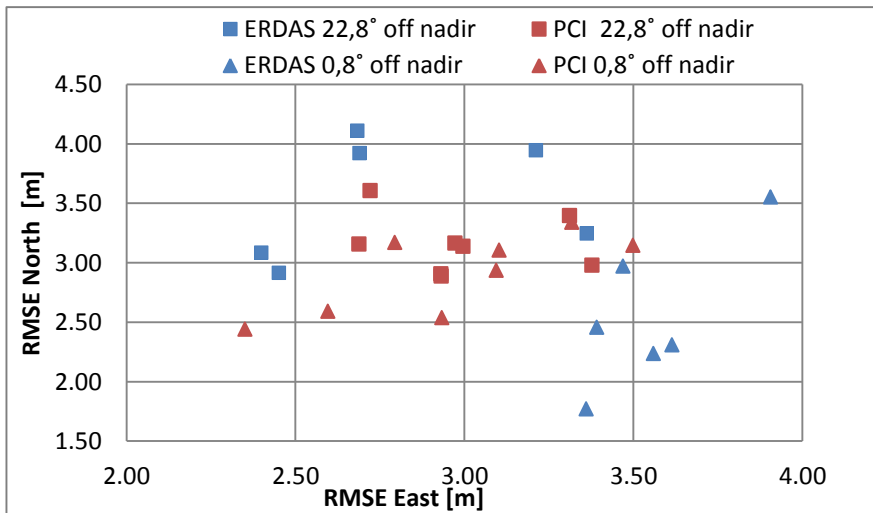
Figure 29 Point representation of planimetric RMSE1D errors measured in the JRC dataset on MSP ortho products, distinguished acording to the off nadir angle and the sofware used.
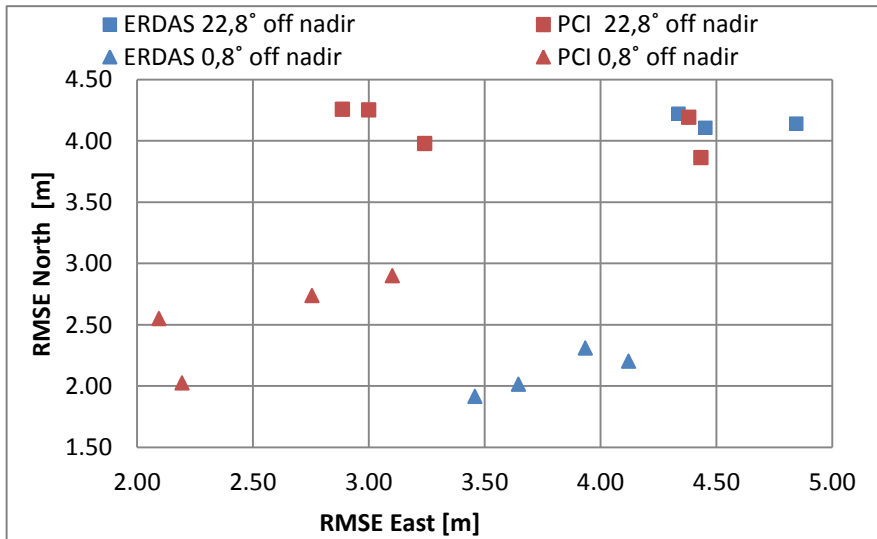
Figure 30 Point representation of planimetric RMSE1D errors measured in the JRC dataset on MSP ortho products, distinguished acording to the off nadir angle and the sofware used.

See the chapter 6.6Discussion on RPC order used for modelling

Figure 31 Graph representation of RMSEs comparison between orthoimages produced using 0 RPC order and 1RPC order, PCI software.

ANNEX 4 EQC by the contractor

All the GCPs, showed in Figure 8, have been considered. Nevertheless, both images have been acquired during winter, when the solar angle is lower. Because of the solar angle, there are many shadows which prevent the correct identification of many GCP in the image.

There were many points which were too close to each other on the ground. In order to have a better spatial distribution of the error measurements, only one point has been selected amongst each group of close GCPs.

The ICPs which were chosen cover most of the images and are distributed as evenly as possible. The following image shows the 20 ICPs which were used to control the image with 22,8º viewing angle.

The following ICPs have been used:

#	ID	Ground position (m) North	Ground position (m) East	Image 22,8	Image 0,8
1	110011	4850032,092	642991,924	x	x
2	440005	4845076,105	645815,166	x	x
3	440008	4843087,455	641527,505	x	x
4	440011	4842244,515	636560,472	x	x
5	440019	4839029,461	642578,110	x	x
6	440021	4837127,366	637082,024	x	x
7	440024	4838510,152	643930,013	x	x
8	G7001	4850123,549	643945,949	x	x
9	G7043	4848795,830	645394,626	x	
10	66007	4845298,880	641804,022	x	x
11	66024	4838276,563	641320,704	x	x
12	66025	4841215,071	641380,518	x	x
13	66026	4840996,065	640049,047	x	x
14	66035	4837489,030	644717,258	x	x
15	66046	4837348,789	641148,671	x	x
16	C1R3	4847236,270	634016,280	x	x
17	C2R4	4843609,870	637829,720	x	x
18	C3R5NEW	4838887,550	640341,360	x	x
19	C3R6	4835621,050	641644,130	x	x
20	550006	4835890,340	649095,120	x	

Table 22: ICP coordinates
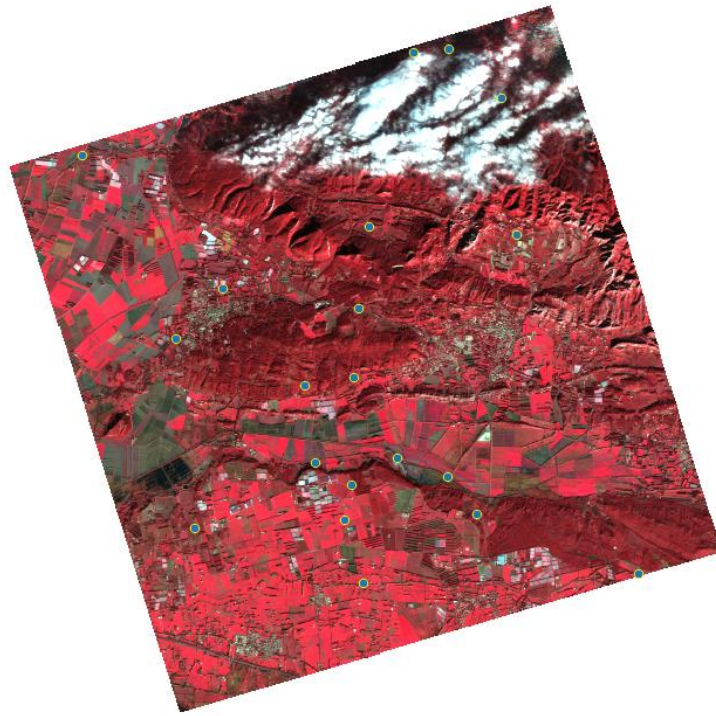
Figure 32: 22,8º image and ICPs

The following image shows the 18 ICPs which were used to control the image with 0,8º viewing angle. The 18 points used for the second image were all used for the first one. One of the ICPs of the first image was outside of the second image footprint and another one had been used as GCP to generate the products, so they were not considered.

Figure 33: 0,8º image and ICPs

Results

In order to measure the deviation of the ICPs located in the image, the Root Mean Square Error is calculated for each product. The following tables show all the results:

ROLL	ERDAS			PCI		
22,8º	RMS X (m)	RMS Y (m)	RMS 2D (m)	RMS X (m)	RMS Y (m)	RMS 2D (m)
PAN/PSH						
3 rpc 0 order	1,530	1,673	2,268	1,672	1,734	2,409
3 rpc 1 order				1,397	1,395	1,975
4 rpc 0 order	1,424	1,665	2,191	1,214	1,489	1,921
4 rpc 1 order	1,343	1,785	2,234	1,370	1,339	1,915
MS4(derived)						
3 rpc 0 order	1,547	1,338	2,046	1,863	1,765	2,566
3 rpc 1 order				1,355	1,545	2,055
4 rpc 0 order	1,013	1,339	1,679	1,449	1,118	1,830
4 rpc 1 order	1,554	1,415	2,102	1,401	1,396	1,978
MS4(located)						
3 rpc 0 order	1,198	1,354	1,808	1,426	1,316	1,941
3 rpc 1 order				1,224	1,672	2,072
4 rpc 0 order	1,148	1,198	1,659	1,132	1,264	1,697
4 rpc 1 order	1,253	1,297	1,804	1,353	1,274	1,858

Table 23: RMSE (m) of 22,8º image

ROLL	ERDAS			PCI		
0,8º	RMS X (m)	RMS Y (m)	RMS 2D (m)	RMS X (m)	RMS Y (m)	RMS 2D (m)
PAN/PSH						
3 rpc 0 order	1,510	1,520	2,142	1,544	1,425	2,101
3 rpc 1 order				1,530	1,055	1,859
4 rpc 0 order	1,450	1,358	1,987	1,329	1,266	1,836
4 rpc 1 order	1,457	1,507	2,096	1,352	1,233	1,829
MS4(derived)						
3 rpc 0 order	1,887	1,638	2,499	1,751	1,364	2,220
3 rpc 1 order				1,462	1,271	1,937
4 rpc 0 order	1,659	1,524	2,253	1,607	1,324	2,083
4 rpc 1 order	1,776	1,422	2,275	1,487	1,112	1,857
MS4(located)						
3 rpc 0 order	0,967	1,515	1,798	1,589	1,586	2,245
3 rpc 1 order				1,651	1,748	2,405
4 rpc 0 order	1,549	1,373	2,070	1,515	1,868	2,405
4 rpc 1 order	1,314	1,576	2,052	1,470	1,905	2,406

Table 24: RMSE (m) of 0,8º image
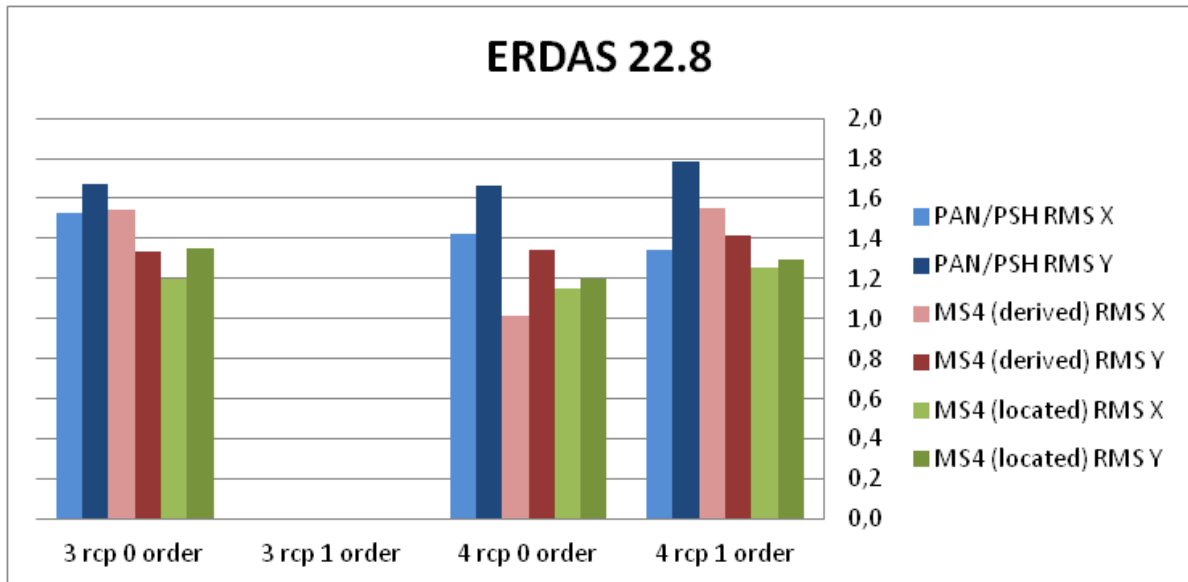
Figure 34: 22,8º image results using ERDAS software
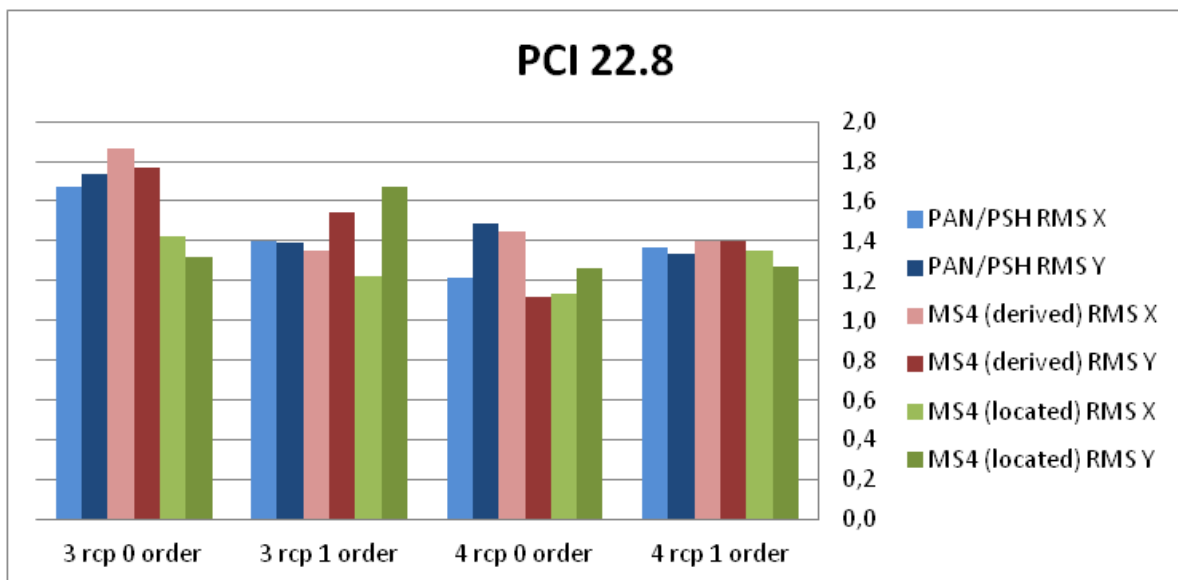
Figure 35: 22,8º image results using PCI software
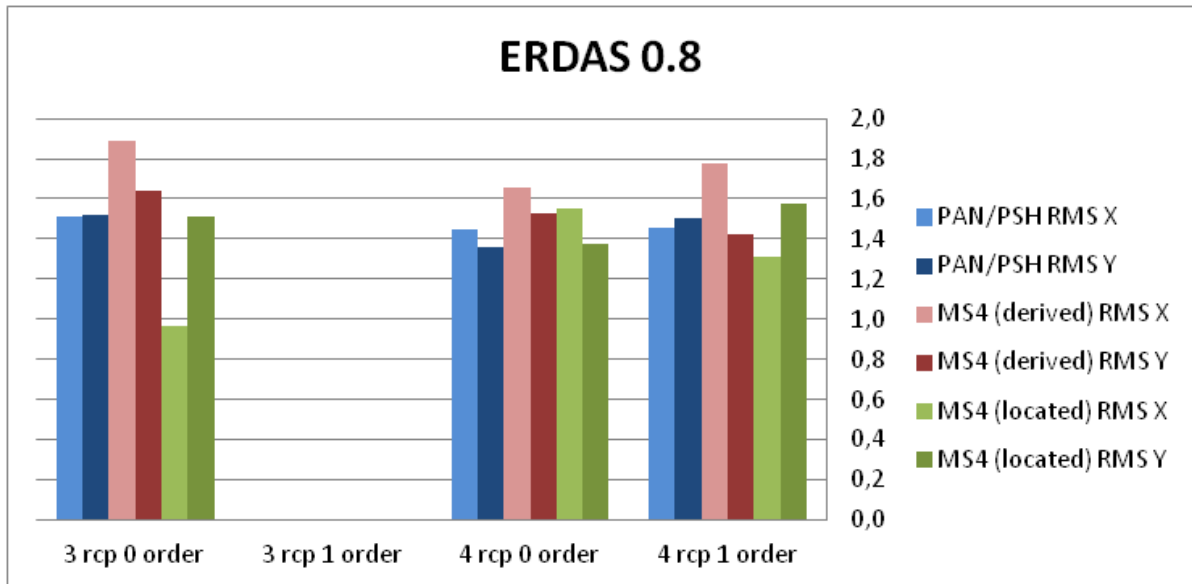
Figure 36: 0,8º image results using ERDAS software
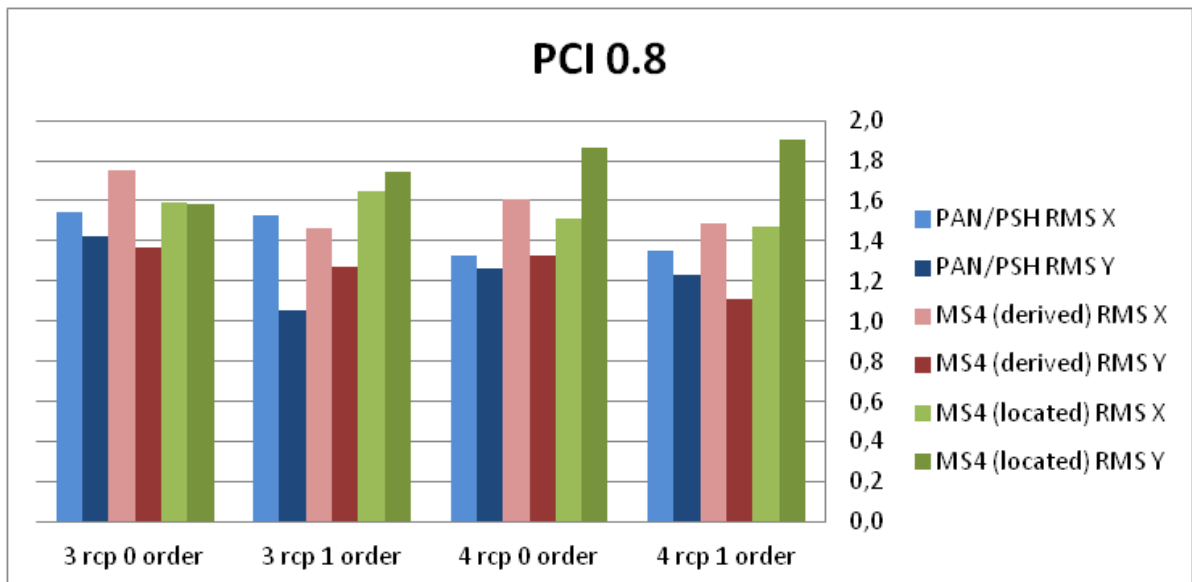
Figure 37: 0,8º image results using PCI software

References

I. Digital Elevation Model over Europe (EU-DEM).
URL:http://www.eea.europa.eu/data-and-maps/data/eu-dem

II. GRAZZINI Jacopo, AASTRAND Paer, External quality control of Pléiades orthoimagery – Part II: Geometric testing and validation of a Pléiades-1B orthoproduct covering Maussane test site. Publications Office of the European Union, 2013. URL: http://publications.jrc.ec.europa.eu/repository/handle/JRC83367

III. GRAZZINI Jacopo; AASTRAND Paer, External quality control of SPOT6 orthoimagery – Geometric benchmarking over Maussane test site for positional accuracy assessment. Publications Office of the European Union, 2013. URL: http://publications.jrc.ec.europa.eu/repository/handle/JRC82314.

IV. JRC IES, HR image acquisition specifications for the CAP checks (CwRS), HR profile-based specifications including HHR profiles (2015, 2016), URL: https://g4cap.jrc.ec.europa.eu/g4cap/Portals/0/Documents/21450_21112015_final.pdf
https://g4cap.jrc.ec.europa.eu/g4cap/Portals/0/Documents/17362.pdf

V. Vincent Parage, Blanka Vajsova, Nathalie Faget, Pär Johan Åstrand, New sensors benchmark report on SPOT 7 Geometric benchmarking over Maussanne test site for CAP purposes. Publications Office of the European Union, 2014. URL: http://publications.jrc.ec.europa.eu/repository/bitstream/JRC93987/spot7_benchmark_final.pdf

VI. D. Kapnias, P. Milenov, and S. Kay, \Guidelines for best practice and quality checking of ortho imagery", Tech. Rep. 48904, JRC IPSC, 2008, URL: http://ies-webarchive-ext.jrc.it/mars/mars/content/download/1231/7140/file/Orthoguidelines_v3_final.pdf

VII. Stefano Cornara, Blanca Altés-Arlandis, Matthias Renard, Stephania Tonetti, Fabrizio Pirondini, Roberto Alacevich, Annalisa Mazzoleni, "Mission Design and Analysis for the DEIMOS-2 Earth Observation Mission," Proceedings of the 63rd IAC (International Astronautical Congress), Naples, Italy, Oct. 1-5, 2012, paper: IAC-12-C1.4.9

VIII. Jorge Gil, Alfredo Romo, Cristina Moclan, Fabrizio Pirondini, Enrique Gonzalez, Jesus Quirce, "The Deimos-2 Mission: Pre and post-launch calibration and data validation," 12th Annual JACIE (Joint Agency Commercial Imagery Evaluation) Workshop, St. Louis, MO, USA, April 16-18, 2013, URL: https://calval.cr.usgs.gov/wordpress/wp-content/uploads/Deimos-2-CALVAL-JACIE-2013-v2.0.pdf

IX. Daniel Hernández, Mercedes Vázquez, Manuel Añón, Esperanza Olivo, Pablo Gallego , Pablo Morillo, Javier Parra, Simone Capraro , Mar Luengo, Beatriz García, Pablo Villacorta, "Environmental testing campaign and verification of satellite Deimos-2 at INTA," Proceedings of the13th European Conference on Spacecraft Structures, Materials & Environmental Testing (SSMET), Braunschweig, Germany, April 1-4, 2014, ESA SP-727

X. Jorge Gil, Alfredo Romo, Cristina Moclan, Fabrizio Pirondini, Diego Lozano, Enrique Gonzalez, Jesus Quirce, "Deimos-2 Radiometric Calibration and Cross-calibration

with Dubaisat-2," Proceedings of JACIE 2014 (Joint Agency Commercial Imagery Evaluation) Workshop, Louisville, Kentucky, March 26-28, 2014, URL: https://calval.cr.usgs.gov/wordpress/wp-content/uploads/14.021_Jorge-Gil_DE-2_DU-2-XCAL-JACIE-2014.pdf

XI. Jorge Gil, Alfredo Romo, Cristina Moclán, Fabrizio Pirondini, "Deimos-2 Post-launch radiometric calibration," JACIE (Joint Agency Commercial Imagery Evaluation)Workshop , Tampa, FL, USA, May 4-8, 2015, URL: https://calval.cr.usgs.gov/wordpress/wp-content/uploads/Jorge-Gil_JACIE-2015_DEIMOS-2-post-launch-radiometric-calibration_fixed.pdf

XII. J. A. González, O. Gonzalez, A. Fernandez, A. Monge, F. Pirondini, A. Ortiz, "gs4EO : An Innovative Solution for Flight Operations Software on Low Cost Missions," SpaceOps 2014, 13th International Conference on Space Operations, Pasadena, CA, USA, May 5-9, 2014, paper: AIAA 2014-1724, URL: http://arc.aiaa.org/doi/pdf/10.2514/6.2014-1724

XIII. J. A. González, C. Fernández, F. Pirondini, "gs4EO: multi-mission user services and receiving stations," Proceedings of the 65th International Astronautical Congress (IAC 2014), Toronto, Canada, Sept. 29-Oct. 3, 2014, paper: IAC-14-B1.4.4

XIV. M. Renard, S. Tonetti, B. Altés-Arlandis, S. Cornara, F. Pirondini, "Fully Automated Mission Planning Tool for DEIMOS-2 Agile Satellite," Proceedings of the 64th International Astronautical Congress (IAC 2013), Beijing, China, Sept. 23-27, 2013, paper: IAC-13-B4.3.2
Herbert J. Kramer, "Deimos-2 Minisatellite Mission", URL: https://directory.eoportal.org/web/eoportal/satellite-missions/d/deimos-2

List of abbreviations and definitions

Acronym	Description
AOI	Area Of Interest
CAP	Common Agriculture Policy
CwRS	Control with Remote Sensing
DEM	Digital Elevation Model
DGPS	Differential Global Positioning System
DMI	Deimos Imaging
EQC	External quality control
EU	European Union
FOV	Field Of Regard
GCP	Ground Control Point
GSD	Ground Sampling Distance
ICP	Independent Check Point
JRC	Joint Research Centre
MS4/MSP	MultiSpectral image (4 bands)
NIR	Near InfraRed
PAN	PANchromatic image
PSH	PanSHarpened image
RMSE	Root Mean Square Error
RMSE 1D	Root Mean Square Error (one dimensional)
RPC	Rational Polynomial Coefficients
VIS	Visible
VHR	Very High Resolution
WV3	WorldView-3

List of figures

List of tables

How to obtain EU publications

Our publications are available from EU Bookshop (http://bookshop.europa.eu),
where you can place an order with the sales agent of your choice.

The Publications Office has a worldwide network of sales agents.
You can obtain their contact details by sending a fax to (352) 29 29-42758.

JRC Mission

As the science and knowledge service of the European Commission, the Joint Research Centre's mission is to support EU policies with independent evidence throughout the whole policy cycle.

EU Science Hub
ec.europa.eu/jrc

@EU_ScienceHub

EU Science Hub - Joint Research Centre

Joint Research Centre

EU Science Hub

Publications Office